Pergamon

Experimental silicate mineral/melt partition coefficients for beryllium and the crustal Be cycle from migmatite to pegmatite

Joseph M. Evensen*† and David London

School of Geology and Geophysics, University of Oklahoma, 100 East Boyd Street, 810 Energy Center, Norman, OK 73019, USA

Abstract—Partition coefficients ($D_{Be}^{mineral/melt}$) for beryllium between hydrous granitic melt and alkali feldspars, plagioclase feldspars, quartz, dark mica, and white mica were determined by experiment at 200 MPa H_2O as a function of temperature (650–900°C), activity of Be in melt (trace levels to beryl saturation), bulk composition, and thermal run direction. At trace levels, Be is compatible in plagioclase of An_{31} (1.84 at 700°C) and muscovite (1.35 at 700°C) but incompatible in biotite (0.39–0.54 from 650–800°C), alkali feldspar (0.38–0.19 from 680–850°C), quartz (0.24 at 800°C), and albite (0.10 at 750°C). The partition coefficients are different at saturation of the melt in beryl: lower in the case of plagioclase of An_{31} (0.89 at 700°C), muscovite (0.87 at 700°C), biotite (0.18–0.08 from 675–800°C), alkali feldspar (0.18–0.14 from 680–700°C), and quartz (0.17–0.08 from 750–800°C), but higher in the case of albite (0.37 at 750°C).

With other data sources, these new partition coefficients were utilized to track, first, the distribution of Be between aluminous quartzofeldspathic source rocks and their anatectic melts, and second, the dispersion or concentration of Be in melt through igneous crystal fractionation of different magma types (e.g., S-type, I-type) up to beryl-saturated granitic pegmatites and, finally, into their hydrothermal aureoles. Among the rock-forming minerals, cordierite, calcic oligoclase, and muscovite (in this order) control the fate of Be because of the compatibility of Be in these phases. In general, beryl-bearing pegmatites can arise only after extended crystal fractionation of large magma batches (to F, fraction of melt remaining, ≤0.05); granitic magmas that originate from cordierite-bearing protoliths or that contain large modal quantities of calcic oligoclase will not achieve beryl saturation at any point in their evolution. *Copyright © 2002 Elsevier Science Ltd*

1. INTRODUCTION

Rock-forming minerals contain negligibly low contents of beryllium. The scarcity of Be (see Table 1) arises from its low cosmogenic abundance (e.g., Goldschmidt, 1954; Goles, 1969). But it is the crystal chemistry of Be that dominates its geologic fate. The principal crystal-chemical factors of Be are (1) its small ionic radius (0.27[4] Å; Shannon, 1976), (2) mixed electron orbital configurations (e.g., Bader et al., 1967) that give rise to appreciable covalency, and (3) a charge density between that of Al and Si but a valence state (2+) that hinders direct substitution for these elements. Within most structures, these characteristics of Be make for a poor fit. Numerous petrologic applications have taken advantage of the fact that Be is strongly incompatible (and thus a reference for other chemical tracers, e.g., Ryan et al., 1996), but at the same time, the incompatibility raises the issue, Where does Be reside? Answering that question entails systematic study of the compatibility of Be in minerals, melts, and fluids. Some such work has been published (e.g., Wood, 1992; Brenan et al., 1998a), but for the crustal rocks that are most enriched in Be—granite systems found in convergent mountain belts and in rift zones within continental tectonic settings (see Table 2)—the database is nonexistent.

1.1. Goals of this Study

In this study, we evaluate the portion of the Be cycle that entails the transfer of Be from mid- to deep-crustal regions of anatexis to the emplacement of evolved plutons and pegmatites at shallow levels of the continental crust. Beryllium contents of melt needed to achieve beryl saturation (± phenakite, Be_2SiO_4; chrysoberyl, $BeAl_2O_4$) have been established (Evensen et al., 1999), and these values provide model limits for the final stages of the petrogenesis of granite–pegmatite systems.

In combination with reported data on cordierite, garnet, and whole-rock compositions of silicic systems, we track the accumulation and depletion of Be in melt by igneous crystal fractionation. Some specific goals of this work are:

- to ascertain which rock-forming minerals are most important in controlling the fate of Be in mineral-melt systems relevant to granite magmatism,
- to establish if there are special mineralogical attributes of sources that predetermine whether their magmas can achieve saturation in beryl, and
- to assess how much crystal fractionation must occur for granitic melts to reach saturation in beryl.

2. EXPERIMENTAL METHODS

2.1. Starting Materials

Powders were formulated by combining mineral components (Table 3) with either a base fraction of a pelite mineral mixture (SP-), a haplogranite mineral mixture (HG-), or glass (synthesized by Corning to 1800°C to the metaluminous composition of the 200-MPa H_2O minimum). Nine Be-poor and seven Be-rich starting mixtures (Table

---

* Author to whom correspondence should be addressed (joey.evensen@exxonmobil.com).
† *Present address:* ExxonMobil Upstream Research Company, PO Box 2189, Houston, TX 77252, USA.

Table 1. Mean beryllium contents of rock-forming minerals in granitoid rocks to pegmatites.

Mineral	Be (ppm)	Range	N	Data Source
K-feldspar	3.1 (0.4)	0.85 to 10	>55	1,2,3
K-alkali feldspar (pegmatitic)	7 (6)	3 to 20	>15	1,4
Na-alkali feldspar	13 (4)	9 to 16	4	2,3
Plagioclase	6.7 (1.2)	1.8 to 20	>30	1,2
Albite	10.3 (1.6)	4 to 20	>13	1
Albite (pegmatitic)	18.1 (2.8)	9 to 40	>10	1,2
Oligoclase	10.7 (0.4)	<1 to 40	260	5
Andesine	4.8 (1.1)	0.4 to 24	>40	5
Quartz	1.2 (0.3)	0.1 to 7.2	>30	1
Quartz (pegmatitic)	2.2 (0.0)	0.5 to 7.35	>25	1
Muscovite	14 (1.9)	11 to 17	>5	2,3
Muscovite (evolved magmatic)	39 (4.2)	31 to 50	>4	1
Muscovite (pegmatitic)	36 (5.8)	12 to 120	106	1,2,4
Lepidolite (pegmatitic)	63 (15.0)	48 to 78	>2	1
Biotite	5.2 (0.8)	0.5 to 11.8		1,2,3
Cordierite (migmatitic)	12.0 (4.31)	7.69 to 16.3	2	6
Cordierite (restite)	7.3 -	-	1	6
Cordierite (evolved magmatic)	7213 (1418)	110 to 10300	7	7,8
Cordierite (pegmatitic)	4724 (1758)	10 to 17700	17	9,10,11,12,13,14
Cordierite (metamorphic)	35 (9.4)	1 to 257	34	15,16
Cordierite (metamorphic, leucocratic)	6775 (464.4)	6000 to 8100	4	17
Garnet	11.5 (2.4)	6 to 20	>5	1
Garnet (pegmatitic)	14.1 (4.3)	0.0 to 50.4	>12	1,18,19
Hornblende	8.6 (1.4)	3.6 to 13.4		1
Alkali amphibole	13.0 -	-	≫1	1

Numbers in parantheses represent precision using reported standard deviations or calculated standard error of the means.

Data sources include: 1. Wuensch and Hörmann, 1978; 2. Kretz et al., 1989; 3. Luecke, 1981; 4. Smeds, 1992; 5. Kosals et al., 1973; 6. Bea et al., 1994a; 7. Schreyer et al., 1979; 8. Gordillo et al., 1985; 9. Černý et al., 1997; 10. Černý and Povondra, 1966; 11. Povondra and Čech, 1978; 12. Povondra et al., 1984; 13. Newton, 1966; 14. Grew et al., 2000; 15. Kalt et al., 1999; 16. Visser et al., 1994; 17. Armbruster and Irouschek, 1983; 18. Gresens, 1966; 19. Evensen, 2001.

4), containing mineral and synthetic components, were used. Starting mixture abbreviations denote the base mineral mixtures (e.g., SP-), the major phase of interest (e.g., Mus), the variation on that mixture (as an integer, e.g., Mus3), and the trace (-C) or high (-Be) beryllium contents in the system, e.g., SP-Mus3-Be. In Be-poor mixtures, beryllium was not added explicitly but by way of trace quantities in the white mica used for the experiments.

Regions of gem quality crystals were selected for crushing, and crystal fragments were microscopically hand sorted to remove impurities before grinding. Starting mixtures were ground on agate under ethanol to a mean grain size of 15 μm and dried in air at 140°C. Powdered components were combined, ground together, dried (140°C), and homogenized overnight in a tumbling mill.

Table 2. Average beryllium contents of crustal rock systems.

Rock Type	Mean Be (ppm)	Range	N	Data Source
Magmatic rocks				
Gabbrodiorite	1 (1)			1
Diorite	2 (0)	2 to 2.8	>5	1,2
Granitic rocks	5 (0)	3 to 6.5	>75	2
S-type granites				
Crd-bearing	0.08 (0.2)	<1 to 1.20	13	4
Crd-absent	5.5 (1.7)	3 to 12	>110	1,3,4
With associated pegmatites	14.0 (8.4)	3 to 64	>50	4
Evolved facies	68.0 (25.9)	11 to 130	>102	4
S-type rhyolites	14.1 (4.8)	4.3 to 37	42	4
A-type granites	6.0			4
A-type rhyolites	14-18 (7.5)	1.8 to 32	101	4
I-type granodiorites	2.9 (0.7)	0.4 to 12.2	>25	1,2
I-type rhyolites	2.6	1.3 to 5.5		4
Metamorphic rocks				
Pelitic schist	4 (0.9)		>10	2,5
Quartzofeldspathic gneiss	3.6 (0.6)		>22	2,6
Amphibolite	2.2 (0.6)		>3	2

Numbers in parantheses represent precision using reported standard deviations or calculated standard error of the means.

Data Sources include: 1. Kozlov, 1969; 2. Wuensch and Hörmann, 1978; 3. Lyakhovich, 1977; 4. Evensen, 2001 and references therein; 5. Luecke, 1981; 6. Grew et al., 2000.

Table 3. Starting materials.

Mineral[a]	albite	adularia	orthoclase	quartz	muscovite-A[b]	muscovite-B	biotite	garnet $Alm_{44}Pyp_{42}Gro_{13}Sps_1$	phenakite	beryl	Haplogranite Glass
Abbreviation	Ab	Or-A	Or-B	Qtz	Mus-A	Mus-B	Bt	Gt	Phn	Brl	HG-glass
No. of analyses	5 (sd)	20 (sd)	166 (se)	6 (sd)	1–3	10 (sd)	96 (sd)	20 (sd)	5 (sd)	7 (sd)	41 (sd)
wt.%											
SiO_2	68.82 (0.16)	64.95 (0.36)	64.05 (0.04)	99.99 (0.03)	51.91 -	47.03 (0.20)	38.83 (0.29)	39.71 (0.26)	54.34 (0.32)	66.00 (0.20)	77.63 (0.59)
TiO_2	nd	nd	nd	nd	0.22 -	0.13 (0.02)	2.05 (0.11)	0.04 (0.02)	0.00	0.06 (0.02)	0.01 (0.01)
Al_2O_3	19.76 (0.05)	18.76 (0.14)	18.67 (0.02)	nd	28.02 -	35.86 (0.16)	11.26 (0.12)	23.20 (0.16)	0.00	19.24 (0.10)	13.03 (0.16)
Fe_2O_3	-	-	0.08 (0.00)	-	3.53 -	-	-	-	-	-	-
FeO	nd	nd	-	nd	0.82[c] -	1.89 (0.02)	18.47 (0.25)	21.26 (0.14)	0.03 (0.02)	0.48 (0.13)	0.02 (0.01)
MnO	nd	nd	nd	nd	0.08 -	0.05 (0.01)	0.83 (0.04)	0.46 (0.02)	0.00	0.00	0.00
ZnO	nd	nd	nd	nd	nd	0.03 (0.02)	0.14 (0.04)	nd	nd	nd	nd
BeO[d]	nd	nd	nd	nd	nd	nd	nd	nd	46.17 (0.99)	13.97 (0.05)	nd
MgO	nd	nd	nd	nd	1.00 -	0.32 (0.01)	14.08 (0.21)	11.46 (0.05)	0.00	0.00	0.01 (0.00)
CaO	0.07 (0.01)	0.01 (0.02)	0.15 (0.00)	nd	0.30 -	0.00	0.00 (0.01)	5.07 (0.04)	0.00	0.00	0.01 (0.01)
BaO	0.06 (0.05)	0.32 (0.04)	0.65 (0.01)	nd	0.09[e] -	0.03 (0.03)	0.10 (0.02)	0.02 (0.02)	0.14 (0.01)	0.03 (0.03)	0.01 (0.01)
Na_2O	11.59 (0.04)	1.21 (0.07)	0.71 (0.01)	nd	1.27 -	0.75 (0.02)	0.56 (0.14)	0.00	0.00	0.08 (0.01)	4.61 (0.11)
K_2O	0.23 (0.02)	14.84 (0.07)	15.41 (0.02)	nd	8.90 -	10.14 (0.05)	9.01 (0.14)	0.00	0.00	0.03 (0.03)	4.79 (0.09)
Rb_2O (ppm)	nd	nd	nd	nd	895[e] -	nd	nd	nd	nd	151[a] (5)	nd
Cs_2O (ppm)	nd	nd	nd	nd	23[e] -	nd	nd	nd	nd	2021[a] (20)	nd
P_2O_5	nd	nd	nd	nd	nd	nd	nd	0.04 (0.01)	nd	nd	0.01 (0.01)
F	nd	nd	nd	nd	nd	0.47 (0.06)	3.67 (0.14)	0.02 (0.03)	nd	nd	0.03 (0.03)
Cl	nd	nd	nd	nd	nd	0.00	0.05 (0.02)	0.01 (0.01)	nd	nd	0.01 (0.01)
H_2O	nd	nd	nd	nd	nd	nd	2.02[e] (0.08)	nd	nd	nd	nd
LOl	-	-	-	-	3.87 -	-	-	-	-	-	-
O=F						−0.20	−1.54	−0.01			−0.01
O=Cl							−0.01				0.00
Total	100.53 (0.18)	100.09 (0.40)	99.72 (0.12)	99.99 (0.03)	100.10 (*0.16*)	98.52 (0.27)	99.52 (0.53)	101.28 (0.35)	100.68 (1.04)	100.11 (0.26)	100.16 (0.63)
H_2O by diff						1.48					

[a] Albite, Copelinha, Minas Gerais, Brazil; adularia, St. Gotthardt, Switzerland; orthoclase, Betroka, Madagascar; quartz, ultrahigh purity, Feldspar Corp., Spruce Pine, NC, USA; muscovite-A, Spruce Pine, NC, USA; muscovite-B, Minas Gerais, Brazil; biotite, Ontario, Canada; garnet, Gore Mountain, NY, USA; phenakite, Espirito Santo, Minas Gerais, Brazil; beryl, Volodarsk, Ukraine; haplogranite glass, 200 MPa minimum anhydrous composition, Corning Glassworks, NY, USA.

[b] Analysed at Activation Laboratories Ltd. (Lancaster, Ontario, Canada) by X-Ray fluorescence (fusion) unless otherwise specified.

[c] Analysed at titration.

[d] Analysed by secondary ion mass spectrometry.

[e] Analysed by instrumental neutron activation analysis.

All other values are from quantitative electron probe microanalysis (with total iron as FeO, except for the orthoclase analysis).

Numbers in parentheses either represent 1 standard deviation (sd) or the standard error (se) of the mean as shown in the header.

Propagated precision is shown for total values; the italicized value represents estimated precision.

Table 4. Starting mixtures.

Mixture	Experiment Type	Constituents (wt.%)											
		Ab	Or-A	Or-B	Qtz	Mus	Mus	Bt	Gt	Al_2O_3	Phn	Brl	HG glass
HG-Or1-C	powder	24.3	23.5	21.5	23.6	7.1							
HG-Or2-C	powder	17.3	15.4	43.0	16.8	7.5							
HG-Or2-Be	powder	27.0	23.9	17.5	26.2						5.4		
HG-Ab1-C	powder	50.6	20.0		22.0	7.4							
HG-Ab2-C	powder	62.8	14.4		15.8	7.0							
HG-Ab1-Be	powder	53.8	19.9		21.8						4.5		
HG-Ab2-Be	powder	66.9	14.2		15.6						3.3		
HG-Qtz3-C	powder	23.3	20.6		49.4	6.7							
SP-Crd1-C	powder	22.7	9.6		26.6	13.1		12.3	15.7				
SP-Crd1-Be	powder	22.7	9.5		26.5	13.1		12.0	15.1		1.1		
SP-Bt2-C	coarse Bt	27.1	11.4		31.8	15.7		11.9		2.1			
SP-Bt2-Be	coarse Bt	22.6	9.4		26.5	12.9		22.1		3.5		3.0	
SP-Mus2-C	coarse Mus	26.7	11.2		31.2	15.4	12.5			3.0			
SP-Mus2-Be	coarse Mus	21.8	9.2		25.6	25.9	11.9			2.7		2.9	
SP-Mus3-C	coarse Mus						50.0						50.0
SP-Mus3-Be	"sandstone"					49.0					1.5		49.5

SP- and HG- in mineral abbreviations denote the base starting composition of "synthetic pelite" or haplogranite, respectively. The designation -Be marks Be-rich mixtures, whereas -C marks Be-poor (control) compositions in which no Be-mineral was added.

Experiment Type consisted of either 100% powdered constituents, powders + coarse mica (circular fragments, 2 mm in diameter), or "sandstone" textures comprised of 100% coarse sand-size grains (~1 mm in diameter).

Analyses of these constituents and definition of their abbreviations are given in Table 1. Dehydrated reagent-grade gibbsite was used for a source of activated Al_2O_3.

2.2. Preparation of Charges

Gold capsules (3 × 20 mm) were cleaned by soaking overnight in bromopropane (25°C) and then by boiling for several hours in nitric acid. Afterwards, a few capsules still contained remnants of the extrusion lubricants used in the fabrication of the tubing; these remnants were removed with polyurethane foam swabs.

Water, followed by powder mixes, was loaded into the central 5 × 3-mm portion of the capsules and sealed by DC-plasma arc welding. All charges contained a slight excess of doubly distilled deionized water needed to slightly oversaturate a melt at 200 MPa and the *T* range investigated (~10 wt.% H_2O). Capsules were weighed before and after welding and again after storage in a drying oven (140°C) to check for leaks. The heating step further allowed for homogenization of water contents throughout the powder before the experimental run.

2.3. Equipment

Experiments were pressurized cold in R-41 and NIMONIC-105 cold-seal reaction vessels using water plus a trace of Immunol as the pressure medium. Pressure was measured with a factory-calibrated Heise bourdon tube gauge; fluctuations of <3 MPa occurred over the course of experiments, with a total estimated uncertainty of ±10 MPa. Experiment durations varied from ~1 to 6 weeks. Temperature was monitored by internal Chromel-Alumel thermocouples with an estimated maximum error of ±5°C. Experiments were quenched isobarically using compressed air jet (5–15°C/s). The fugacity of oxygen within capsules was regulated by diffusion of H_2 across the metal capsule, and the fO_2 is estimated to be slightly below NNO (Huebner, 1971) at run conditions. Following quench, capsules were weighed to check for leaks, punctured, and the presence of free water was recorded. Capsules were heated in a drying oven and reweighed to verify loss of free water (~25% of total added water). All capsules gain minor weight during experiments by diffusion of Ni-metal (from vessels and filler rods) into precious-metal capsule walls, although none of the experimental products reported here (including biotite) suffered from detectable contamination by Ni.

2.4. Run Pathways and Experimental Strategy

Forward-direction experiments (prograde to run temperatures of 700–850°C, designated F in Tables 5, 6, 7) promoted concurrent melting and new crystal growth. Reverse-direction experiments (designated R in Tables 5, 6, 7) were preconditioned by melting at 50 to 150°C above the final *T* of the experiment, followed by isobaric quench to room temperature, then run up (forward) to final temperature (in the range of 675–800°C). This pathway utilized glass to increase reaction rates on the reversed step to avoid metastable persistence of granitic melt on direct cooling. These reverse-direction experiments induced crystal growth from melts that were substantially supersaturated in the components of the crystalline phases at the final run *T*.

Variants of the first three mixtures (Table 4: HG-Or-, HG-Ab-, and HG-Qtz) change in proportion of quartz, orthoclase, or albite with temperature to be within the respective feldspar or quartz liquidus stability field at 200 MPa (Tuttle and Bowen, 1958). Growth of K-rich alkali feldspar was achieved in reversed experiments and by the muscovite breakdown reaction,

$$KAl_3Si_3O_{10}(OH)_2 + SiO_2 = KAlSi_3O_8 + Al_2SiO_5 + H_2O \quad (1)$$

muscovite + quartz (m) = K-feldspar + aluminosilicate (m) + water

in forward experiments. Albite (Ab) was precipitated in reversed experiments, whereas andesine was grown via the reaction of the grossular component of garnet in melt,

$$Ca_3Al_2Si_3O_{12} + Al_2SiO_5 + SiO_2 = CaAl_2Si_2O_8 \quad (2)$$
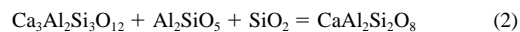
grossular + aluminosilicate (m) + quartz = anorthite

Dark mica was grown in reversed experiments and by the breakdown of garnet in melt with or without biotite seeds (added coarse biotite) in forward experiments,

$$(Mg,Fe)_3Al_2Si_3O_{12} + KAlSi_3O_8 + H_2O = K(Mg,Fe)_3AlSi_3O_{10}(OH)_2$$
$$+ Al_2SiO_5 + 2SiO_2 \quad (3)$$
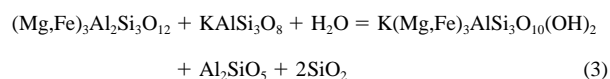
garnet + orthoclase + water = biotite + aluminosilicate + quartz

and by decomposition of a ferroan component in the starting white mica (Mus-2, Table 4) into melt. White mica was grown in reversed experiments and by the decomposition of a garnet component in potassic, peraluminous melt with or without muscovite seeds,

Table 5a. Coexisting K-rich alkali feldspar - glass compositional pairs.

	Trace Be Contents									
Run	BeP-49		BeP-64		BeP-47		BeP-30		BeP-31	
Mixture	SP-Mus2-C		SP-Mus3-C		SP-Mus2-C		HG-Or-C		HG-Or-C	
Prec. Path/Duration (d)	730-F (21)		740-F (1)		730-F (21)		800-F (14)		850-F (5)	
Final Path/Duration (d)	675-R (36)		680-R (31)		700-R (28)		750-R (21)		800-R (15)	
Crystalline Products	K-Afs,Mus,Als,Cor,Bt,Mt		K-Afs,(Mus)		K-Afs,Mus,Als,Cor,Bt,Mt		K-Afs		K-Afs	
Analysis of	K-Afs	Glass	K-Afs	Glass	K-Afs	Glass	K-Afs	Glass	K-Afs	Glass
No. analyses, QEPMA	10	11	8	10	9	8	11	10	12	10
No. analyses, SIMS	1	1	1	2	1	1	1	5	1	1
Measure of precision	(sd)	(sd)	(se)	(sd)	(sd)	(sd)	(se)	(sd)	(se)	(sd)
wt.%										
SiO_2	64.24 (0.67)	69.45 (0.84)	64.63 (0.68)	72.23 (0.87)	63.29 (0.39)	69.12 (0.72)	64.95 (0.43)	70.21 (0.63)	64.83 (0.11)	68.83 (1.27)
TiO_2	0.01 (0.01)	0.03 (0.01)	0.02 (0.01)	0.01 (0.01)	0.01 (0.01)	0.03 (0.01)	0.01 (0.00)	0.02 (0.02)	0.02 (0.01)	0.03 (0.02)
B_2O_3 (ppm)[1]	19.50 -	203.12 -	28.20 -	74.69 (48.22)	6.89 -	164.24 -	13.66 -	47.99 (3.50)	18.07 -	55.79 -
Al_2O_3	18.99 (0.37)	13.45 (0.39)	19.65 (0.27)	12.86 (0.39)	19.47 (0.46)	13.76 (0.30)	18.59 (0.29)	12.96 (0.32)	18.48 (0.09)	14.51 (0.27)
FeO	0.10 (0.02)	0.34 (0.03)	0.07 (0.02)	0.21 (0.02)	0.09 (0.02)	0.37 (0.02)	0.06 (0.01)	0.33 (0.02)	0.09 (0.01)	0.35 (0.02)
MnO	0.01 (0.01)	0.03 (0.01)	0.01 (0.00)	0.01 (0.01)	0.00 (0.01)	0.04 (0.01)	0.01 (0.01)	0.01 (0.01)	0.00 (0.00)	0.01 (0.01)
MgO	0.01 (0.00)	0.18 (0.01)	0.01 (0.00)	0.03 (0.01)	0.01 (0.00)	0.19 (0.01)	0.00 (0.00)	0.08 (0.01)	0.01 (0.00)	0.09 (0.01)
NiO	0.01 (0.00)	nd	0.00 (0.00)	nd	0.00 (0.00)	nd	0.01 (0.00)	nd	0.00 (0.00)	nd
ZnO	nd	nd	0.01 (0.00)	nd	nd	nd	nd	nd	nd	nd
BeO (ppm)[1]	1.22 -	17.14 -	1.73 -	4.55 (0.39)	0.24 -	13.76 -	1.35 -	5.27 (0.19)	1.00 -	5.16 -
CaO	0.02 (0.01)	0.36 (0.10)	0.03 (0.01)	0.02 (0.03)	0.02 (0.01)	0.24 (0.03)	0.01 (0.00)	0.15 (0.02)	0.03 (0.00)	0.28 (0.05)
BaO	0.49 (0.04)	0.01 (0.01)	nd	0.01 (0.01)	0.84 (0.16)	0.02 (0.02)	1.20 (0.02)	0.02 (0.02)	0.68 (0.05)	0.03 (0.04)
Li_2O (ppm)[1]	127.20 -	428.64 -	59.75 -	497.66 (32.24)	26.90 -	326.59 -	29.03 -	76.34 (4.67)	14.19 -	78.74 -
Na_2O	2.47 (0.08)	3.11 (0.13)	3.93 (0.11)	3.74 (0.18)	2.15 (0.07)	3.18 (0.11)	1.98 (0.02)	3.25 (0.14)	1.37 (0.01)	2.76 (0.09)
K_2O	12.70 (0.08)	4.62 (0.08)	10.79 (0.18)	4.00 (0.09)	13.01 (0.16)	5.18 (0.20)	13.31 (0.02)	5.79 (0.14)	14.11 (0.18)	7.46 (0.12)
Rb_2O (ppm)[1]	262.07 -	279.80 -	83.28 -	105.24 (3.29)	227.26 -	243.56 -	184.29 -	226.09 (5.78)	274.73 -	355.86 -
Cs_2O (ppm)[1]	3.26 -	9.86 -	1.48 -	3.73 (2.47)	1.59 -	9.04 -	3.30 -	8.91 (1.05)	0.65 -	9.36 -
P_2O_5	nd	0.10 (0.03)	nd	0.04 (0.02)	nd	0.06 (0.04)	nd	0.08 (0.01)	nd	0.08 (0.04)
F	0.03 (0.03)	0.11 (0.04)	0.03 (0.01)	0.15 (0.07)	0.05 (0.04)	0.08 (0.07)	0.02 (0.02)	0.02 (0.02)	0.05 (0.02)	0.02 (0.03)
Cl	0.01 (0.00)	0.00 (0.00)	0.01 (0.00)	0.01 (0.01)	0.01 (0.01)	0.01 (0.01)	nd	0.01 (0.00)	nd	0.01 (0.00)
O=F	−0.01 (0.01)	−0.04 (0.02)	−0.01 (0.01)	−0.06 (0.03)	−0.02 (0.02)	−0.03 (0.03)	−0.01 (0.01)	−0.01 (0.01)	−0.02 (0.01)	−0.01 (0.01)
O=Cl	0.00 (0.00)	0.00 (0.00)	0.00 (0.00)	0.00 (0.00)	0.00 (0.00)	0.00 (0.00)		0.00 (0.00)		0.00 (0.00)
total	99.11 (0.35)	91.84 (0.68)	99.19 (0.64)	93.32 (0.66)	98.95 (0.64)	92.33 (0.51)	100.16 (0.64)	92.96 (0.81)	99.69 (0.64)	94.49 (1.44)
H_2O by diff		8.16		6.68		7.67		7.04		5.51
ASI		1.23 (0.02)		1.20 (0.03)		1.21 (0.03)		1.09 (0.03)		1.10 (0.03)
$D_{Be}^{Afs/MELT}$	0.07		0.38		0.02		0.26		0.19	
structural cations/18O										
Si	2.97 (0.03)		2.96 (0.04)		2.94 (0.03)		2.99 (0.03)		2.99 (0.02)	
Al	1.04 (0.02)		1.06 (0.02)		1.07 (0.03)		1.01 (0.02)		1.01 (0.01)	
Li	0.00		0.00		0.00		0.00		0.00	
Na	0.22 (0.01)		0.35 (0.01)		0.19 (0.01)		0.18 (0.00)		0.12 (0.00)	
K	0.75 (0.01)		0.63 (0.01)		0.77 (0.01)		0.78 (0.01)		0.83 (0.01)	
Rb	0.00		0.00		0.00		0.00		0.00	
Ca	0.00		0.00		0.00		0.00		0.00	
Ba	0.01 (0.00)		nd		0.02 (0.00)		0.02 (0.00)		0.01 (0.00)	
Total	4.99 (0.04)		5.00 (0.04)		4.99 (0.04)		4.98 (0.03)		4.97 (0.02)	
mol% An	0.08 (0.00)		0.14 (0.00)		0.08 (0.00)		0.04 (0.00)		0.14 (0.00)	
mol% Ab	22.56 (0.93)		35.58 (1.37)		19.71 (0.81)		17.99 (0.49)		12.67 (0.34)	
mol% Or	76.37 (1.92)		64.25 (1.92)		78.58 (2.20)		79.71 (1.99)		85.84 (2.41)	
mol% celsian	0.91 (0.08)		nd		1.56 (0.30)		2.21 (0.07)		1.26 (0.10)	

[1] Analysis by SIMS. All other data are derived from QEPMA.

Mineral abbreviations include: K-Afs, K-rich alkali feldspar; Na-Afs, Na-rich alkali feldspar; Pl, plagioclase; Ab, albite; Qtz, quartz; Mus, muscovite; Bt, biotite; Als, aluminosilicate; Mt, magnetite; Cor, corundum; Crd, cordierite; Brl, beryl; Phn, phenakite; Cbr, chrysoberyl.

Parantheses around mineral abbreviations indicate relict (vs. new) occurrence.

Table 5b. Coexisting K- and Na-rich alkali feldspar - glass compositional pairs.

	K-alkali feldspar, beryl-saturated				Na-alkali feldspar, trace Be contents		Na-alkali feldspar, beryl-saturated	
Run	BeP-76		BeP-12		BeP-35		BeP-32	
Mixture	SP-Mus3-Be		HG-Or-Be		HG-Ab-C		HG-Ab-Be	
Prec. Path/Duration (d)	740-F (1)		800-F (6)		750-F (21)		750-F (21)	
Final Path/Duration (d)	680-R (31)		750-R (30)		700-R (28)		700-R (28)	
Crystalline Products	K-Afs,Cor,Bt,Mt,(Mus),(Phn)		K-Afs,(Phn)		Na-Afs		Na-Afs,(Phn)	
Analysis of	K-Afs	Glass	K-Afs	Glass	Na-Afs	Glass	Na-Afs	Glass
No. analyses, QEPMA	11	10	19	12	13	10	17	10
No. analyses, SIMS	1	1	1	3	1	1	1	3
Measure of precision	(se)	(sd)	(se)	(sd)	(se)	(sd)	(se)	(sd)
wt.%								
SiO_2	64.57 (0.28)	70.89 (0.81)	62.40 (0.09)	68.90 (1.33)	67.64 (0.25)	70.76 (1.11)	67.01 (0.10)	72.10 (0.53)
TiO_2	0.01 (0.00)	0.02 (0.02)	0.01 (0.00)	0.01 (0.01)	0.01 (0.01)	0.02 (0.01)	0.01 (0.01)	0.01 (0.01)
B_2O_3 (ppm)[1]	619.36 -	78.15 -	8.10 -	24.93 (0.96)	18.91 -	54.75 -	2.70 -	46.00 (0.26)
Al_2O_3	19.26 (0.09)	13.02 (0.25)	19.45 (0.06)	12.27 (0.35)	19.49 (0.16)	13.00 (0.32)	20.06 (0.23)	12.63 (0.33)
FeO	0.06 (0.01)	0.23 (0.02)	0.02 (0.00)	0.03 (0.01)	0.06 (0.01)	0.28 (0.03)	0.01 (0.01)	0.02 (0.01)
MnO	0.01 (0.00)	0.01 (0.01)	0.00	0.01 (0.01)	0.00	0.00	0.01 (0.00)	0.01 (0.01)
MgO	0.01 (0.00)	0.06 (0.01)	0.00	0.00	0.00	0.05 (0.01)	0.00	0.00
NiO	0.00	nd	0.00	nd	0.00	nd	0.01 (0.00)	nd
ZnO	0.01 (0.00)	nd	nd	nd	nd	nd	nd	nd
BeO (ppm)[1]	67.48 -	383.95 -	274.42 -	2002.86 (45.25)	5.97 -	21.36 -	190.11 -	1374.20 (392.61)
CaO	0.01 (0.00)	0.02 (0.03)	0.00	0.05 (0.02)	0.13 (0.01)	0.16 (0.03)	0.11 (0.01)	0.17 (0.05)
BaO	nd	0.01 (0.01)	3.33 (0.08)	0.15 (0.04)	0.24 (0.07)	0.00 (0.01)	0.33 (0.03)	0.02 (0.03)
Li_2O (ppm)[1]	45.77 -	727.38 -	2.07 -	12.98 (1.25)	41.93 -	126.47 -	6.41 -	44.28 (0.05)
Na_2O	3.31 (0.05)	3.56 (0.11)	1.89 (0.01)	3.39 (0.10)	9.03 (0.11)	4.31 (0.06)	9.43 (0.10)	4.58 (0.14)
K_2O	11.83 (0.05)	4.25 (0.06)	12.55 (0.05)	5.72 (0.13)	3.37 (0.12)	3.77 (0.12)	2.24 (0.15)	3.62 (0.11)
Rb_2O (ppm)[1]	1197.39 -	213.76 -	117.94 -	162.34 (0.30)	42.97 -	114.97 -	4.40 -	84.11 (2.29)
Cs_2O (ppm)[1]	24.51 -	8.06 -	2.91 -	11.68 (0.79)	7.51 -	10.30 -	3.34 -	35.45 (0.47)
P_2O_5	nd	0.05 (0.03)	nd	0.02 (0.01)	nd	0.11 (0.03)	nd	0.09 (0.03)
F	0.05 (0.02)	0.16 (0.05)	0.02 (0.01)	0.05 (0.04)	0.03 (0.01)	0.05 (0.03)	0.04 (0.02)	0.01 (0.02)
Cl	0.00	0.00	nd	0.01 (0.00)	nd	0.01 (0.00)	nd	0.01 (0.01)
O=F	−0.02	−0.07	−0.01	−0.02	−0.01	−0.02	−0.02	−0.01
O=Cl	0.00	0.00		0.00		0.00		0.00
total	99.32 (0.26)	92.37 (0.58)	99.72 (0.20)	90.80 (1.66)	100.01 (0.60)	92.54 (1.25)	99.25 (0.64)	93.42 (0.73)
H_2O by diff		7.63		9.20		7.46		6.58
ASI		1.21 (0.03)		1.03 (0.03)		1.13 (0.03)		1.07 (0.04)
$D_{Be}^{Afs/MELT}$	0.18		0.14		0.28		0.14	
structural cations/18O								
Si	2.96 (0.02)		2.93 (0.01)		2.99 (0.02)		2.97 (0.02)	
Al	1.04 (0.01)		1.08 (0.00)		1.02 (0.01)		1.05 (0.01)	
Li	0.00		0.00		0.00		0.00	
Na	0.29 (0.00)		0.17 (0.00)		0.77 (0.01)		0.81 (0.01)	
K	0.69 (0.00)		0.75 (0.00)		0.19 (0.01)		0.13 (0.01)	
Rb	0.00		0.00		0.00		0.00	
Ca	0.00		0.00		0.01 (0.00)		0.01 (0.00)	
Ba	nd		0.06 (0.00)		0.00 (0.00)		0.01 (0.00)	
Total	4.99 (0.02)		4.99 (0.01)		4.98 (0.03)		4.97 (0.03)	
mol% An	0.04 (0.00)		0.02 (0.00)		0.61 (0.01)		0.53 (0.01)	
mol% Ab	29.75 (0.25)		17.46 (0.08)		79.43 (1.08)		85.49 (1.36)	
mol% Or	69.85 (0.58)		76.27 (0.35)		19.52 (0.27)		13.38 (0.21)	
mol% celsian	-		6.21 (0.15)		0.43 (0.13)		0.60 (0.06)	

[1] Analysis by SIMS. All other data are derived from QEPMA.

Mineral abbreviations include: K-Afs, K-rich alkali feldspar; Na-Afs, Na-rich alkali feldspar; Pl, plagioclase; Ab, albite; Qtz, quartz; Mus, muscovite; Bt, biotite; Als, aluminosilicate; Mt, magnetite; Cor, corundum; Crd, cordierite; Brl, beryl; Phn, phenakite; Cbr, chrysoberyl.

Parantheses around mineral abbreviations indicate relict (vs. new) occurrence.

Table 5c. Coexisting albite - glass and andesine - glass compositional pairs.

	albite, trace Be contents		albite, beryl-saturated		andesine, trace Be contents				andesine, beryl-saturated	
Run	BeP-36		BeP-33		BeP-56		BeP-60		BeP-53	
Mixture	HG-Ab-C		HG-Ab-Be		SP-Crd1-C		SP-Crd1-C		SP-Crd1-Be	
Prec. Path/Duration (d)	800-F (13)		800-F (13)							
Final Path/Duration (d)	750-R (21)		750-R (21)		700-F (27)		700-F (27)		700-F (27)	
Crystalline Products	Ab		Ab, (Phn)		Crd,Pl,Mt,Bt,Qtz		Crd,Qtz,Pl,Bt,Mt		Crd,Pl,Bt,Brl,Mt,Qtz	
Composition of	Ab	Glass	Ab	Glass	An32	Glass	An31	Glass	An31	Glass
No. analyses, QEPMA	14	10	10	10	9	11	19	10	9	11
No. analyses, SIMS	2	1	1	3	2	2	3	3	2	2
Measure of precision	(sd)	(sd)	(se)	(sd)	(se)	(sd)	(se)	(sd)	(se)	(sd)
wt.%										
SiO_2	67.12 (0.40)	65.87 (0.89)	67.70 (0.20)	67.07 (1.07)	59.11 (0.32)	70.95 (0.60)	61.13 (0.66)	70.83 (1.04)	61.60 (0.40)	71.45 (0.56)
TiO_2	0.01 (0.01)	0.02 (0.02)	0.01 (0.00)	0.00 (0.01)	0.01 (0.01)	0.05 (0.01)	0.01 (0.01)	0.01 (0.01)	0.01 (0.01)	0.05 (0.02)
B_2O_3 (ppm)[1]	1.56 (0.25)	77.00 -	45.53 -	43.54 -	78.99 (1.48)	92.58 (2.42)	14.32 (0.70)	99.83 (0.77)	92.16 (2.64)	95.32 (0.58)
Al_2O_3	19.95 (0.27)	15.26 (0.44)	20.18 (0.13)	14.59 (0.32)	24.99 (0.10)	12.80 (0.25)	24.38 (0.49)	12.12 (0.18)	24.45 (0.14)	12.14 (0.13)
FeO	0.08 (0.01)	0.25 (0.02)	0.01 (0.00)	0.03 (0.01)	0.20 (0.02)	0.62 (0.05)	0.21 (0.02)	0.36 (0.03)	0.29 (0.03)	0.57 (0.03)
MnO	0.00	0.01 (0.01)	0.01 (0.00)	0.01 (0.01)	0.02 (0.01)	0.09 (0.01)	0.03 (0.01)	0.10 (0.01)	0.01 (0.01)	0.06 (0.01)
MgO	0.00	0.05 (0.00)	0.00	0.00	0.00	0.21 (0.01)	0.02 (0.01)	0.15 (0.02)	0.00	0.15 (0.01)
NiO	0.01 (0.00)	nd	0.01 (0.00)	nd	0.01 (0.01)	nd	0.00	nd	0.00	nd
BeO (ppm)[1]	1.11 (0.01)	10.94 -	1249.08 -	3367.25 -	2.45 (0.67)	1.45 (0.07)	1.19 (0.29)	0.60 (0.05)	889.28 (2.97)	1003.15 (11.10)
CaO	0.30 (0.03)	0.15 (0.02)	0.18 (0.02)	0.10 (0.03)	6.30 (0.10)	0.85 (0.04)	6.26 (0.23)	0.61 (0.09)	6.04 (0.06)	0.92 (0.08)
BaO	0.30 (0.05)	0.04 (0.03)	0.14 (0.03)	0.04 (0.03)	0.01 (0.01)	0.06 (0.03)	0.03 (0.02)	nd	0.03 (0.04)	0.04 (0.03)
Li_2O (ppm)[1]	12.31 (0.31)	111.04 -	40.09 -	42.10 -	379.30 (1.14)	451.82 (9.00)	116.08 (4.70)	408.56 (8.00)	331.64 (15.40)	435.90 (1.31)
Na_2O	10.50 (0.10)	6.37 (0.13)	10.63 (0.04)	6.63 (0.18)	7.35 (0.06)	3.21 (0.10)	7.49 (0.20)	3.04 (0.11)	7.55 (0.02)	3.27 (0.15)
K_2O	1.11 (0.07)	2.97 (0.06)	0.73 (0.04)	2.39 (0.07)	0.35 (0.02)	3.31 (0.10)	0.53 (0.07)	3.61 (0.10)	0.48 (0.04)	3.58 (0.15)
Rb_2O (ppm)[1]	2.92 (0.01)	80.92 -	41.13 -	49.76 -	90.31 (1.13)	104.33 (3.01)	7.66 (0.01)	134.08 (5.00)	96.00 (2.20)	114.46 (0.89)
Cs_2O (ppm)[1]	0.00 -	17.46 -	19.10 -	27.69 -	7.91 (2.47)	8.75 (0.00)	1.88 (0.00)	10.60 (2.00)	10.89 (0.59)	8.43 (0.39)
P_2O_5	nd	0.10 (0.02)	nd	0.12 (0.08)	nd	0.12 (0.05)	nd	0.04 (0.03)	nd	0.11 (0.07)
F	0.02 (0.01)	0.02 (0.02)	0.02 (0.01)	0.05 (0.04)	0.02 (0.02)	0.18 (0.04)	0.02 (0.01)	0.21 (0.05)	0.00	0.22 (0.07)
Cl	nd	0.01 (0.01)	nd	0.01 (0.00)	nd	0.01 (0.00)	0.00	0.00	nd	0.01 (0.01)
O=F	−0.01	−0.01	−0.01	−0.02	−0.01	−0.08	−0.01	−0.09	0.00	−0.09
O=Cl	0.00	0.00		0.00		0.00	0.00	0.00		
total	99.37 (0.57)	91.13 (1.29)	99.74 (0.64)	91.37 (1.26)	98.42 (0.34)	92.45 (0.63)	100.12 (0.40)	91.06 (1.19)	100.62 (0.59)	92.65 (0.64)
H_2O by diff		8.87		8.63		7.55		8.94		7.35
ASI		1.09 (0.03)		1.07 (0.04)		1.21 (0.03)		1.19 (0.03)		1.10 (0.03)
$D_{Be}^{Ab/MELT}$	0.10		0.37		1.69 (0.47)		1.99 (0.51)		0.89	
Structural cations/18O										
Si	2.97 (0.02)		2.71 (0.02)		2.67 (0.02)		2.72 (0.03)		2.72 (0.02)	
Al	1.04 (0.02)		0.95 (0.01)		1.33 (0.01)		1.28 (0.03)		1.27 (0.01)	
Li	0.00		0.00		0.01		0.00		0.01	
Na	0.90 (0.01)		0.83 (0.01)		0.64 (0.01)		0.65 (0.02)		0.65 (0.00)	
K	0.06 (0.00)		0.04 (0.00)		0.02 (0.00)		0.03 (0.00)		0.03 (0.00)	
Rb	0.00		0.00		0.00		0.00		0.00	
Ca	0.01 (0.00)		0.01 (0.00)		0.31 (0.01)		0.30 (0.01)		0.29 (0.00)	
Be	0.01 (0.00)		0.00		0.00 (0.00)		0.00 (0.00)		0.00 (0.00)	
Total	4.99 (0.03)		4.54 (0.02)		4.98 (0.02)		4.97 (0.04)		4.96 (0.03)	
mol% An	1.43 (0.03)		0.89 (0.01)		31.47 (0.29)		30.59 (0.77)		29.77 (0.39)	
mol% Ab	91.69 (2.27)		94.59 (1.18)		66.40 (0.61)		66.25 (1.66)		67.36 (0.88)	
mol% Or	6.35 (0.11)		4.27 (0.05)		2.09 (0.02)		3.11 (0.08)		2.79 (0.04)	
mol% celsian	0.52 (0.10)		0.25 (0.00)		0.02 (0.01)		0.05 (0.03)		0.06 (0.06)	

[1] Analysis by SIMS. All other data are derived from QEPMA.

Mineral abbreviations include: K-Afs, K-rich alkali feldspar; Na-Afs, Na-rich alkali feldspar; Pl, plagioclase; Ab, albite; Qtz, quartz; Mus, muscovite; Bt, biotite; Als, aluminosilicate; Mt, magnetite; Cor, corundum; Crd, cordierite; Brl, beryl; Phn, phenakite; Cbr, chrysoberyl.

Parantheses around mineral abbreviations indicate relict (vs. new) occurrence.

Table 6. Coexisting quartz - glass compositional pairs.

	trace Be contents				beryl-saturated	
Run	BeP-40		Be-711		Be-751	
Mixture	HG-Qtz-C					
Prec. Path/Duration (d)	850-F (6)		800-F (6)		850-F (21)	
Final Path/Duration (d)	800-R (14)		750-R (30)		800-R (36)	
Crystalline Products	Qtz		Qtz, Brl, Cbr		Qtz, Brl, Cbr	
Analysis of	Qtz	Glass	Qtz	Glass	Qtz	Glass
No. analyses, QEPMA	10	10	11	12	10	12
No. analyses, SIMS	1	1	2	3	1	2
Measure of precision	(se)	(sd)	(se)	(sd)	(se)	(sd)
wt.%						
SiO_2	98.80 (0.34)	77.68 (0.78)	99.31 (0.38)	74.73 (0.43)	99.51 (0.23)	75.86 (0.42)
TiO_2	0.01 (0.00)	0.02 (0.02)	0.00 (0.00)	nd	0.01 (0.00)	nd
B_2O_3 (ppm)2	6.31 -	23.35 -	4.73 -	nd	2.13 -	nd
Al_2O_3	0.08 (0.01)	9.66 (0.24)	0.16 (0.01)	11.69 (0.18)	0.07 (0.03)	10.81 (0.10)
FeO	0.01 (0.01)	0.26 (0.01)	0.00	nd	0.00	nd
MnO	0.01 (0.00)	0.01 (0.01)	0.00	nd	0.00	nd
MgO	0.00	0.06 (0.01)	0.00	nd	0.00	nd
NiO	0.01 (0.00)	nd (0.04)	0.00	nd	0.01 (0.00)	nd
ZnO	0.02 (0.02)	nd	nd	nd	nd	nd
BeO (ppm)2	0.96 -	3.95 -	78.90 -	452.00 (13.00)	70.59 -	982.00 (6.00)
CaO	0.01 (0.00)	0.17 (0.04)	0.00	0.03 (0.01)	0.00	0.02 (0.02)
BaO	0.01 (0.00)	0.06 (0.04)	0.01 (0.01)	nd	0.02 (0.01)	nd
Li_2O (ppm)2	6.16 -	67.74 -	0.77 -	nd	1.83 -	nd
Na_2O	0.01 (0.00)	2.76 (0.11)	0.01 (0.01)	3.16 (0.12)	0.02 (0.01)	2.78 (0.07)
K_2O	0.01 (0.00)	3.68 (0.11)	0.01 (0.00)	3.56 (0.12)	0.01 (0.00)	3.11 (0.08)
Rb_2O (ppm)2	17.39 -	72.22 -	1.72 -	nd	3.93 -	nd
Cs_2O (ppm)2	0.66 -	7.06 -	1.90 -	nd	3.63 -	nd
P_2O_5	nd	0.10 (0.04)	nd	nd	nd	nd
F	0.05 (0.02)	0.06 (0.04)	0.07 (0.05)	nd	0.03 (0.01)	nd
Cl	0.00	0.01 (0.00)	0.00	nd	0.01 (0.00)	nd
O=F	−0.02	−0.03	−0.03		−0.01	
O=Cl	0.00	0.00	0.00		0.00	
total	99.00 (0.30)	94.51 (0.58)	99.57 (0.37)	93.19 (1.66)	99.67 (0.21)	92.67 (0.68)
H_2O by diff		5.49		6.81		7.33
ASl		1.09 (0.03)		1.28 (0.03)		1.35 (0.02)
$D_{Be}^{Qtz/MELT}$	0.24		0.17		0.07	

[1] Major element glass chemistry taken from Evensen et al. (1999).
[2] Analysis by SIMS. All other data are derived from QEPMA.

$$2 (Mg,Fe)_3Al_2Si_3O_{12} + 3\ KAlSi_3O_8 + 3\ H_2O =$$

$$garnet + orthoclase + water =$$

$$KAl_3Si_3O_{10}(OH)_2 + 2\ K(Mg,Fe)_3AlSi_3O_{10}(OH)_2 + Al_2SiO_5 + 5\ SiO_2 \qquad (4)$$
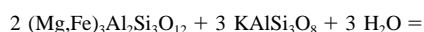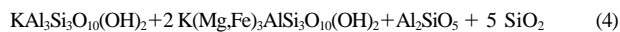
$$muscovite + biotite + aluminosilicate + quartz$$

Finally, new quartz was crystallized in reversed experiments.

In Be-rich experiments, two reactions were utilized to buffer the activity of Be in melt. Saturation in beryl was achieved using the phenakite decomposition reaction,

$$3\ Be_2SiO_4 + 2\ Al_2SiO_5 + 7\ SiO_2 \rightarrow 2\ Be_3Al_2Si_6O_{18} \qquad (5)$$
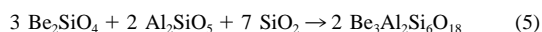
$$phenakite + aluminosilicate\ (m) + quartz \rightarrow beryl$$

In strongly peraluminous melts, saturation in chrysoberyl was achieved by reaction of beryl,

$$Be_3Al_2Si_6O_{18} + 2\ KAl_3Si_3O_{10}(OH)_2 \rightarrow 3\ BeAl_2O_4 + 2\ KAlSi_3O_8$$

$$+ 6\ SiO_2 + H_2O \qquad (6)$$
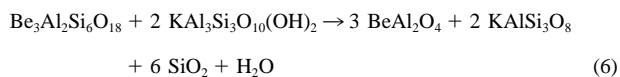
$$beryl + muscovite \rightarrow chrysoberyl + K\text{-}feldspar + quartz\ (m) + water$$

Each starting mixture successfully produced the crystalline phase(s) of interest with target crystals amendable to analysis (see below).

2.5. Derivation of Partition Coefficients and Analytical Strategy

Zonation in crystal products was found to only occur in reverse-direction experiments in which early growth of cordierite and feldspar (possibly dark mica, though not observed) was armored by the latter growth of a compositionally distinct zone at that lower T step. Where single zonation occurred, crystal cores and rims were analysed and reported using the methods below (e.g., see Table 5), but only the compositions from the outermost region of crystal rims, whether zoned or not, were used for mineral/melt partitioning calculations. We interpret the outermost rims of new crystals to represent the most likely compositions of crystals in equilibrium with melt. Figure 1 schematically illustrates this approach.

Table 7a. Coexisting dark mica - glass compositional pairs..

trace Be contents

Run	BeP-60 Bt	BeP-60 Glass	Run 8+61 Bt	Run 8+61 Glass1	BeP-58 Bt	BeP-58 Glass	Run 5+151 Bt	Run 5+151 Glass1	BeP-47 Bt	BeP-47 Glass	BeP-20 Bt	BeP-20 Glass
Mixture	SP-Crd-1				SP-Crd-1				SP-Mus2-C		SP-Crd1-C	
Prec. Path/Duration (d)							750-F (21)		730-F (22)		850-F (6)	
Final Path/Duration (d)	700-F (26)		700-F (28)		800-F (14)		650-R (36)		700-R (29)		700-R (28)	
Crystalline Products	Crd,Bt,Mt,Qtz,Pl				Crd,Bt,Mt				Kfs,Cor,Mus,Als,Bt,Mt		Crd,Bt,Mt	
Analysis of	Bt	Glass	Bt	Glass1	Bt	Glass	Bt	Glass1	Bt	Glass	Bt	Glass
No. analyses, QEPMA	8	10	6	10	10	11	10	20	8	8	10	8
No. analyses, SIMS	2	>3	2	2	1	2	2	2	2	1	1	2
Measure of precision	(se)	(sd)	(se)	(sd)	(se)	(sd)	(se)	(sd)	(sd)	(sd)	(se)	(sd)
wt.%												
SiO_2	40.42 (1.56)	70.83 (1.04)	35.52 (1.50)	64.78 (0.54)	42.14 (0.76)	70.01 (0.53)	37.25 (0.63)	63.94 (0.20)	41.12 (2.61)	69.12 (0.72)	43.65 (1.82)	70.82 (0.63)
TiO_2	2.01 (0.16)	0.01 (0.01)	1.89 (0.10)	nd	0.91 (0.27)	0.12 (0.02)	1.80 (0.08)	0.09 (0.01)	0.51 (0.05)	0.03 (0.01)	0.74 (0.04)	0.04 (0.01)
B_2O_3 (ppm)[2]	41.80 (6.86)	99.83 (0.77)	110.32 (8.37)	231.08 (1.00)	3.70 -	79.54 (0.32)	131.80 (5.70)	298.25 (7.28)	60.86 (10.08)	164.24 -	54.49 -	123.80 (1.93)
Al_2O_3	12.09 (0.37)	12.12 (0.18)	22.46 (0.55)	116.83 (0.79)	17.09 (0.80)	13.12 (0.25)	20.87 (0.23)	15.84 (0.08)	20.89 (0.49)	13.76 (0.30)	16.76 (0.45)	12.47 (0.18)
FeO	13.47 (1.98)	(0.03)	15.66 (0.74)	0.94 (0.22)	7.31 (0.24)	0.81 (0.05)	16.00 (0.27)	0.74 (0.06)	9.48 (0.70)	0.37 (0.02)	10.33 (0.39)	0.67 (0.13)
MnO	0.55 (0.13)	0.10 (0.01)	0.35 (0.02)	0.07 (0.01)	0.18 (0.01)	0.11 (0.01)	0.33 (0.01)	0.07 (0.00)	0.09 (0.01)	0.04 (0.01)	0.23 (0.01)	0.09 (0.01)
MgO	16.40 (1.20)	0.15 (0.02)	6.69 (0.41)	0.20 (0.08)	18.91 (0.33)	0.52 (0.01)	8.13 (0.15)	0.16 (0.02)	12.47 (1.00)	0.19 (0.01)	14.87 (0.67)	0.22 (0.01)
NiO	0.01 (0.02)	nd	0.57 (0.12)	nd	0.01 (0.00)	nd	0.01 (0.01)	0.04 (0.03)	0.47 (0.06)	nd	0.01 (0.00)	nd
ZnO	0.02 (0.02)	nd	nd	nd	0.06 (0.01)	nd	0.02 (0.01)	nd	0.01 (0.01)	nd	0.03 (0.01)	nd
BeO (ppm)[2]	0.28 (0.02)	0.60 (0.05)	22.47 (0.86)	53.41 (2.20)	2.33 -	5.00 (0.20)	28.73 (1.05)	68.70 (0.25)	6.82 (0.20)	13.76 -	2.62 -	3.39 (0.14)
CaO	0.03 (0.02)	0.61 (0.09)	0.02 (0.04)	0.54 (0.04)	0.11 (0.01)	1.06 (0.09)	0.06 (0.02)	0.83 (0.01)	0.02 (0.01)	0.24 (0.03)	0.12 (0.03)	0.96 (0.05)
BaO	0.10 (0.04)	nd	3.29 (0.33)	0.14 (0.04)	0.25 (0.03)	0.05 (0.03)	0.10 (0.01)	0.27 (0.03)	0.25 (0.03)	0.02 (0.02)	0.23 (0.04)	0.05 (0.05)
Li_2O (ppm)[2]	188.19 (3.26)	408.56 (8.03)	3153.32 (138.63)	4720.40 (158.02)	72.35 -	434.39 (3.23)	5088.59 (10.03)	7182.40 (31.11)	194.05 (8.12)	326.59 -	121.84 -	383.37 (2.02)
Na_2O	0.27 (0.03)	3.04 (0.11)	0.38 (0.04)	2.88 (0.14)	0.90 (0.03)	3.14 (0.12)	0.33 (0.02)	1.95 (0.02)	0.51 (0.11)	3.18 (0.11)	0.81 (0.03)	3.30 (0.09)
K_2O	9.07 (0.26)	3.61 (0.10)	7.85 (0.31)	4.30 (0.12)	7.96 (0.03)	3.36 (0.15)	8.25 (0.13)	3.28 (0.04)	7.95 (0.39)	5.18 (0.20)	7.80 (0.21)	2.77 (0.06)
Rb_2O (ppm)[2]	331.57 (4.55)	134.08 (4.60)	3214.15 (498.36)	3120.61 (10.02)	358.58 -	109.69 (0.55)	2608.85 (459.98)	4166.39 (12.96)	293.59 (14.63)	243.56 -	376.29 -	101.95 (0.00)
Cs_2O (ppm)[2]	10.80 (2.60)	10.60 (2.12)	2309.36 (61.27)	4032.61 (100.88)	4.06 -	11.82 (2.00)	4420.26 (161.09)	7777.36 (183.71)	5.40 (0.83)	9.04 -	48.23 -	10.70 (1.31)
P_2O_5	nd	0.04 (0.03)	nd	nd	nd	0.12 (0.03)	nd	nd	nd	0.06 (0.04)	nd	0.04 (0.02)
F	2.83 (0.28)	0.21 (0.05)	2.67 (0.12)	1.10 (0.09)	2.27 (0.12)	0.19 (0.07)	2.98 (0.03)	1.74 (0.04)	0.88 (0.10)	0.08 (0.07)	1.91 (0.08)	0.18 (0.07)
Cl	0.05 (0.01)	0.00	0.00 (0.00)	nd	0.02 (0.00)	0.01 (0.01)	0.01 (0.00)	nd	0.01 (0.00)	0.01 (0.01)	0.01 (0.00)	0.01 (0.01)
O=F	−1.19	−0.09	−1.13	−0.46	−0.96	−0.08	−1.25	−0.04	−0.37	−0.03	−0.80	−0.07
O=Cl	−0.01	0.00	0.00		0.00	0.00	0.00		0.00	0.00	0.00	0.00
total	96.17 (0.37)	90.70 (1.19)	97.11 (0.96)	92.54 (0.61)	97.20 (0.82)	92.58 (0.64)	96.12 (0.60)	90.85 (0.68)	94.34 (0.78)	92.33 (0.51)	96.76 (0.48)	91.60 (0.75)
H_2O by diff	3.83	9.30	2.89		2.80	7.42	3.88	9.15	5.66	7.67	3.24	8.40
ASI		1.19 (0.03)		1.38 (0.03)		1.21 (0.05)		1.45 (0.02)		1.21 (0.03)		1.21 (0.02)
Mg#	67.6 (1.2)		42.7 (2.2)		81.8 (0.8)		47.0 (0.9)		69.9 (1.4)		71.5 (2.8)	
$D_{Be}^{Bt/MELT}$	0.47 (0.05)		0.42 (0.02)		0.47		0.42 (0.02)		0.50		0.77	

Structural cations/12O

	BeP-60	Run 8+61	BeP-58	Run 5+151	BeP-47	BeP-20
Si	2.84 (0.11)	2.81 (0.12)	2.68 (0.05)	2.42 (0.04)	2.91 (0.19)	2.79 (0.12)
Ti	0.11 (0.01)	0.11 (0.01)	0.04 (0.01)	0.09 (0.00)	0.03 (0.00)	0.04 (0.00)
Al	1.00 (0.03)	1.08 (0.03)	1.28 (0.06)	1.49 (0.02)	1.06 (0.03)	1.17 (0.03)
[4]total	3.94 (0.11)	4.00 (0.13)	4.00 (0.08)	4.00 (0.05)	4.00 (0.19)	4.00 (0.12)
Al	0.00	0.00	0.00 (0.00)	0.11 (0.00)	0.68 (0.01)	0.09 (0.00)
Fe	0.79 (0.12)	1.04 (0.05)	0.39 (0.01)	0.87 (0.02)	0.56 (0.04)	0.55 (0.02)
Mn	0.03 (0.01)	0.02 (0.00)	0.01 (0.00)	0.02 (0.00)	0.01 (0.00)	0.01 (0.00)
Mg	1.72 (0.13)	0.79 (0.05)	1.79 (0.03)	0.79 (0.02)	1.32 (0.11)	1.42 (0.06)
Li	0.01 -	0.10 (0.00)	0.00	0.13 (0.00)	0.01 -	0.00
[6]total	2.55 (0.17)	1.95 (0.07)	2.20 (0.04)	1.92 (0.02)	2.57 (0.11)	2.08 (0.07)
Be	0.00 (0.00)	0.10 (0.01)	0.01 (0.00)	0.00 (0.00)	0.01 (0.00)	0.01 (0.00)
Na	0.04 (0.00)	0.06 (0.01)	0.11 (0.00)	0.04 (0.00)	0.07 (0.01)	0.10 (0.00)
K	0.81 (0.02)	0.79 (0.03)	0.65 (0.01)	0.68 (0.01)	0.72 (0.04)	0.64 (0.02)
Rb	0.00	0.02	0.00	0.01 (0.00)	0.00	0.00
Cs	0.00	0.01	0.00	0.01 (0.00)	0.00	
[12]total	0.85 (0.02)	0.98 (0.03)	0.76 (0.01)	0.75 (0.01)	0.80 (0.04)	0.74 (0.02)
Total cations	7.34 (0.21)	6.93 (0.15)	6.96 (0.09)	6.67 (0.05)	7.36 (0.22)	6.82 (0.14)
F	0.63 (0.06)	0.669 (0.03)	0.46 (0.02)	0.61 (0.01)	0.20 (0.02)	0.39 (0.02)

[1] From Icenhower and London (1995).

[2] Analysis by SIMS. All other data are derived from QEPMA.

J. M. Evensen and D. London

Table 7b. Coexisting dark mica - glass compositional pairs (continued)..

	Trace Be Contents				beryl-saturated					
Run	BeP-45		BeP-46		BeP-41		BeP-54		BeP-43	
Mixture	SP-Bt2-C		SP-Bt2-C		SP-Bt2-Be		SP-Crd1-Be		SP-Bt2-Be	
Prec. Path/Duration (d)	800-F (15)		850-F (6)		750-F (21)				850-F (6)	
Final Path/Duration (d)	750-R (23)		800-R (14)		700-R (28)		750-F (27)		800-R (14)	
Crystalline Products	Crd,Bt,Mt		Bt,Mt		Crd,Br,Bt,Mt		Crd,Brl,Bt,Mt		Crd,Brl,Bt,Mt	
Analysis of	Bt	Glass	Bt	Glass	Bt	Glass	Bt	Glass	Bt	Glass
No. analyses, QEPMA	10	10	12	10	14	11	19	12	19	10
No. analyses, SIMS	1	1	1	1	1	2	1	2	1	1
Measure of precision	(se)	(sd)	(se)	(sd)	(se)	(sd)	(se)	(sd)	(se)	(sd)
wt.%										
SiO$_2$	40.14 (0.95)	70.56 (0.65)	45.79 (1.69)	69.54 (0.80)	38.99 (0.52)	68.92 (0.49)	43.93 (1.87)	70.32 (0.41)	40.67 (0.91)	70.04 (0.33)
TiO$_2$	1.64 (0.09)	0.07 (0.02)	1.29 (0.06)	0.17 (0.03)	1.98 (0.04)	0.08 (0.02)	1.57 (0.19)	0.03 (0.02)	1.48 (0.05)	0.16 (0.03)
B$_2$O$_3$ (ppm)[1]	64.44 -	149.42 -	74.26 -	99.21 -	213.05 -	98.05 (1.77)	70.97 -	88.55 (3.00)	138.24 -	131.70 -
Al$_2$O$_3$	16.15 (0.88)	13.82 (0.20)	15.91 (0.46)	13.78 (0.21)	15.89 (1.32)	13.35 (0.07)	12.97 (0.83)	12.73 (0.14)	16.18 (0.13)	13.99 (0.24)
FeO	8.73 (0.26)	0.57 (0.04)	6.89 (0.50)	0.79 (0.04)	12.26 (0.62)	0.44 (0.03)	10.03 (1.96)	0.57 (0.04)	8.58 (0.35)	0.78 (0.04)
MnO	0.29 (0.01)	0.15 (0.01)	0.27 (0.01)	0.17 (0.02)	0.36 (0.02)	0.07 (0.02)	0.30 (0.03)	0.09 (0.02)	0.28 (0.01)	0.13 (0.01)
MgO	17.87 (0.23)	0.35 (0.01)	15.93 (0.71)	0.42 (0.01)	14.19 (0.69)	0.10 (0.01)	17.19 (1.10)	0.23 (0.01)	18.51 (0.38)	0.33 (0.01)
NiO	0.09 (0.02)	nd	0.10 (0.02)	nd	0.27 (0.24)	nd	0.01 (0.00)	nd	0.20 (0.06)	nd
ZnO	nd	nd	nd	nd	nd	nd	nd	nd	nd	nd
BeO (ppm)[1]	4.67 -	12.10 -	7.14 -	12.77 -	90.03 -	511.10 (2.87)	621.17 -	1523.02 (9.80)	147.33 -	1890.58 -
CaO	0.00 (0.00)	0.19 (0.03)	0.02 (0.00)	0.20 (0.07)	0.01 (0.00)	0.16 (0.09)	0.14 (0.06)	1.04 (0.10)	0.00 (0.00)	0.24 (0.08)
BaO	0.24 (0.04)	0.02 (0.02)	0.26 (0.04)	0.04 (0.02)	0.33 (0.06)	0.05 (0.05)	0.11 (0.03)	0.05 (0.03)	0.40 (0.03)	0.06 (0.04)
Li$_2$O (ppm)[1]	371.56 -	628.79 -	520.34 -	856.42 -	628.06 -	613.05 (22.39)	233.12 -	405.33 (11.41)	458.89 -	802.09 -
Na$_2$O	0.59 (0.04)	3.29 (0.16)	0.74 (0.03)	3.31 (0.12)	0.49 (0.09)	3.19 (0.07)	0.47 (0.08)	3.25 (0.12)	0.68 (0.02)	3.24 (0.14)
K$_2$O	8.92 (0.11)	4.14 (0.11)	7.83 (0.23)	4.31 (0.11)	8.92 (0.20)	4.60 (0.09)	7.73 (0.71)	3.72 (0.12)	9.02 (0.06)	4.80 (0.14)
Rb$_2$O (ppm)[1]	168.73 -	182.88 -	189.76 -	151.00 -	418.13 -	153.21 (3.55)	159.48 -	125.65 (12.22)	441.67 -	185.89 -
Cs$_2$O (ppm)[1]	8.08 -	12.86 -	13.74 -	8.65 -	41.26 -	34.99 (2.00)	14.13 -	9.17 (2.62)	59.49 -	38.42 -
P$_2$O$_5$	nd	0.09 (0.02)	nd	0.10 (0.04)	nd	0.06 (0.03)	nd	0.09 (0.03)	nd	0.08 (0.02)
F	3.44 (0.17)	0.47 (0.07)	3.25 (0.13)	0.54 (0.05)	3.05 (0.20)	0.50 (0.02)	2.65 (0.23)	0.28 (0.07)	3.79 (0.16)	0.66 (0.05)
Cl	nd	0.01 (0.01)	nd	0.02 (0.01)	nd	0.01 (0.01)	0.03 (0.01)	0.01 (0.01)	nd	0.01 (0.01)
O=F	−1.45 (0.07)	−0.20 (0.03)	−1.37 (0.06)	−0.23 (0.02)	−1.28 (0.08)	−0.21	−1.12	−0.12	−1.59 (0.16)	−0.28 (0.02)
O=Cl		0.00 (0.00)		0.00 (0.00)		0.00	−0.01	0.00		0.00 (0.00)
total	96.72 (0.18)	93.64 (0.81)	96.99 (0.37)	93.25 (0.95)	95.59 (0.34)	91.46 (0.63)	96.14 (0.69)	92.51 (0.47)	98.33 (0.28)	94.56 (0.53)
H$_2$O by diff	3.28		3.01		4.41	8.54	3.86	7.49	1.67	
ASI		1.32 (0.03)		1.28 (0.04)		1.24 (0.03)		1.12 (0.03)		1.24 (0.04)
Mg#	77.9 (0.6)		79.9 (0.7)		66.7 (0.5)		74.8 (14.8)		78.8 (0.6)	
D$_{Be}$ $^{Bt/MELT}$	0.39		0.56		0.18		0.41		0.08	
Structural cations/12O										
Si	2.71 (0.06)		3.00 (0.11)		2.73 (0.04)		2.99 (0.13)		2.69 (0.06)	
Ti	0.08 (0.00)		0.06 (0.00)		0.10 (0.00)		0.08 (0.01)		0.07 (0.00)	
Al	1.21 (0.07)		0.93 (0.02)		1.17 (0.09)		0.92 (0.05)		1.23 (0.01)	
Be	0.00		0.00		0.00		0.01		0.00	
[4]total	4.00 (0.09)		4.00 (0.11)		4.00 (0.10)		4.00 (0.14)		4.00 (0.06)	
Al	0.08 (0.00)		0.30 (0.00)		0.14 (0.01)		0.12 (0.01)		0.03 (0.00)	
Fe	0.49 (0.01)		0.38 (0.03)		0.72 (0.04)		0.57 (0.11)		0.48 (0.02)	
Mn	0.02 (0.00)		0.02 (0.00)		0.02 (0.00)		0.02 (0.00)		0.02 (0.00)	
Mg	1.80 (0.02)		1.56 (0.07)		1.48 (0.07)		1.74 (0.11)		1.83 (0.04)	
Li	0.01		0.01		0.02		0.01		0.01	
[6]total	2.40 (0.03)		2.26 (0.08)		2.38 (0.08)		2.46 (0.16)		2.36 (0.04)	
Ba	0.01 (0.00)		0.01 (0.00)		0.01 (0.00)		0.00 (0.00)		0.01 (0.00)	
Na	0.08 (0.01)		0.09 (0.00)		0.07 (0.01)		0.06 (0.01)		0.09 (0.00)	
K	0.77 (0.01)		0.66 (0.02)		0.80 (0.02)		0.67 (0.06)		0.76 (0.01)	
Rb	0.00		0.00		0.00		0.00		0.00	
[12]total	0.85 (0.01)		0.76 (0.02)		0.87 (0.02)		0.74 (0.06)		0.86 (0.01)	
Total cations	7.25 (0.10)		7.02 (0.14)		7.26 (0.13)		7.19 (0.22)		7.22 (0.08)	
F	0.74 (0.04)		0.67 (0.03)		0.67 (0.04)		0.57 (0.05)		0.79 (0.03)	

[1] From Icenhower and London (1995).

Table 7c. Coexisting white mica - glass compositional pairs.

	trace Be contents		beryl-saturated	
Run	BeP-47		BeP-52	
Mixture	SP-Mus2-C		SP-Mus2-Be	
Prec. Path/Duration (d)	730-F (21)		750-F (21)	
Final Path/Duration (d)	700-R (31)		700-R (28)	
Crystalline Products	K-Afs,Mus		K-Afs,Mus,Als,Cor,Bt,Mt	
Analysis of	Mus (sd)	Glass (sd)	Mus (se)	Glass (sd)
No. analyses, QEPMA	8	10	9	8
No. analyses, SIMS	1	3	1	1
wt.%				
SiO_2	64.63 (1.35)	72.23 (0.87)	63.03 (0.36)	69.12 (0.72)
TiO_2	0.02 (0.01)	0.01 (0.01)	0.01 (0.00)	0.03 (0.01)
B_2O_3 (ppm)[1]	533.07 -	171.63 -	204.71 -	250.40 -
Al_2O_3	19.65 (0.54)	12.86 (0.39)	18.47 (0.11)	13.76 (0.30)
FeO	0.07 (0.05)	0.21 (0.02)	0.09 (0.01)	0.37 (0.02)
MnO	0.01 (0.01)	0.01 (0.01)	0.00 (0.00)	0.04 (0.01)
MgO	0.01 (0.01)	0.03 (0.01)	0.01 (0.00)	0.19 (0.01)
NiO	0.00 (0.00)	nd	0.01 (0.00)	nd
ZnO	0.01 (0.01)	nd	nd	nd
BeO (ppm)[1]	19.43 -	14.38 -	755.02 -	869.44 -
CaO	0.03 (0.03)	0.02 (0.03)	0.02 (0.00)	0.24 (0.03)
BaO	nd	0.01 (0.01)	0.94 (0.10)	0.02 (0.02)
Li_2O (ppm)[1]	444.98 -	341.29 -	385.18 -	353.75 -
Na_2O	3.93 (0.23)	3.74 (0.18)	2.16 (0.05)	3.18 (0.11)
K_2O	10.79 (0.35)	4.00 (0.09)	12.98 (0.10)	5.18 (0.20)
Rb_2O (ppm)[1]	224.95 -	254.51 -	316.84 -	359.96 -
Cs_2O (ppm)[1]	7.45 -	9.45 -	35.20 -	42.70 -
P_2O_5	nd	0.04 (0.02)	nd	0.06 (0.04)
F	0.03 (0.03)	0.15 (0.07)	0.05 (0.03)	0.08 (0.07)
Cl	0.01 (0.01)	0.01 (0.01)	nd	0.01 (0.01)
O=F	−0.01 (0.01)	−0.06 (0.03)	−0.02 (0.01)	−0.03 (0.03)
O=Cl	0.00 (0.00)	0.00 (0.00)		0.00 (0.00)
total	99.30 (0.18)	93.33 (0.81)	97.92 (0.18)	92.44 (0.81)
H_2O by diff	0.70		2.08	
ASl		1.21 (0.03)		1.21 (0.03)
$D_{Be}^{Mus/MELT}$	1.35		0.87	
Structural cations/12O				
Si	4.06 (0.09)		4.08 (0.02)	
B	0.01		0.00	
Be	0.00		0.01	
[4]total	4.06 (0.09)		4.08 (0.02)	
Al	1.45 (0.04)		1.41 (0.01)	
Fe	0.00		0.01	
Li	0.01		0.01	
[6]total	1.46 (0.04)		1.42 (0.01)	
Na	0.45 (0.03)		0.27 (0.01)	
K	0.87 (0.03)		1.07 (0.01)	
Rb	0.00		0.00	
Cs	0.00		0.00	
[12]total	1.32 (0.04)		1.34 (0.01)	
total cations	6.83 (0.10)		6.85 (0.03)	
F	0.01 (0.00)		0.01 (0.01)	
mol% Mus	64.36 (4.32)		79.79 (5.35)	
mol% paragonite	35.64 (2.39)		20.21 (1.35)	

[1] From Icenhower and London (1995).

3. ANALYTICAL METHODS

3.1. Quantitative Electron Probe Microanalysis (QEPMA)

All major and minor element oxide constituents of mineral and glass products, except H, Li, Be, B, Rb, and Cs, were analyzed using wavelength-dispersive spectroscopy on a Cameca SX-50 electron microprobe at the University of Oklahoma. QEPMA utilized crystalline and glass standards with TAP, PET, LIF, and layered composite (PC1) diffraction devices. Operating conditions for hydrous glass analyses used a two-beam condition (2- and 20-nA regulated currents method)
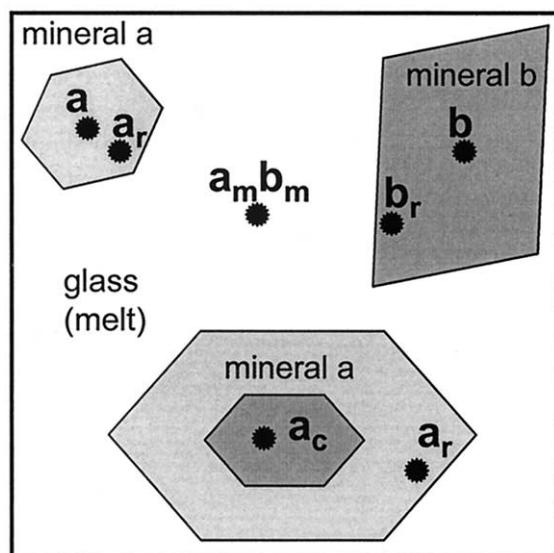
Fig. 1. Schematic illustration of the analytical approach to mineral and glass pairs for the calculation of $D_{Be}^{mineral/melt}$ values. For every mineral, multiple intercrystalline and intracrystalline analyses were acquired (dark spots) along with analyses of crystal-free glass pools (open space) away from crystal interfaces (spot analysis at a_m, b_m). In reverse-direction experiments, in which crystals became singly zoned, crystal core (a_c) and rim (a_r) compositions were reported, but only rim data were used to calculate partition coefficients. In all other experiments, a similar approach was taken: If no zoning was present and crystal core compositions (a,b) converged with rim data (a_r, b_r), then the mean values were used for calculation; otherwise, only rim data were used (e.g., b_r/b_m). Care was taken in glass analyses to avoid potential compositional boundary layers near crystals, although these were never documented.

with a 20-μm spot size in which Na and Al were analyzed first (and concurrently) to inhibit beam-induced migration effects (Morgan and London, 1996). Analyses of minerals were conducted at 20 nA, 20 kV, and a spot size of 3 to 5 μm. Counting times for all elements varied between 20 and 30 s. Data were reduced using the PAP (Pouchou and Pichoir, 1985) matrix correction procedure. Detection levels, taken at 3σ above mean background, were <500 ppm for most elements. Analyses of similar Be-rich experiments indicate that Be is not lost to the capsule metal (Evensen and Meeker, 1997).

Secondary and backscattered electron imaging (BSEI) allowed images to be collected as 1024 × 1024 pixelized data. Micrographs were processed (following Russ, 1999) using low-pass or median filtering for reduction of noise.

3.2. Secondary Ion Mass Spectrometry (SIMS)

Samples were analysed by SIMS using a Cameca Instruments IMS 3f at Arizona State University at Tempe. A mass-filtered $^{16}O^-$ primary beam was accelerated through a potential of 12.5 kV with a beam current of 1.0 nA. The focused spot size varied from 15 to 5 μm, and sputtered secondary ions were accelerated through a potential of 4.5 kV. Targets were mapped in advance and verified by imaging a combination of ^7Li, ^9Be, ^{23}Na, ^{26}Mg, ^{27}Al, ^{41}K, and ^{56}Fe before analysis. Data were carefully inspected (optically by BSEI using compositional indicators) for possible contamination of the analytical volume (e.g., from inclusions or crossing of crystal boundaries). Data suspect to contamination were not reported.

The interference of $^{27}Al^{3+}$ (8.99384 amu) on ^9Be (9.01219 amu) is the most important concern in SIMS microanalysis of Be (Hervig, 2002). The yield of ^9Be is substantially greater than the $^{27}Al^{3+}$ species when Be contents are high (e.g., Evensen, 2001), resulting in negligible interference (no correction is required). Grew et al. (1998) observed

that trivalent Al begins to affect the analysis when Be contents are <~30 ppm. Therefore, before and after each analysis, the mass-collecting position was distinguished from $^{27}Al^{3+}$ and aligned to the ^9Be peak. Individual analyses consisted of collecting intensities on the following sequence of isotopes: ^{30}Si, ^7Li, ^9Be, ^{11}B, ^{85}Rb, ^{133}Cs, and ^{30}Si (collected twice). Integration times were sufficiently long to achieve a counting precision of at least 3%. The count rates were normalized to that for Si and then to the silica abundance in the sample (derived from QEPMA).

A standard working curve for SIMS was calibrated for the analysis of Li, Be, B, Rb, and Cs using glass standards and one crystalline standard. Three synthetic granitic glasses doped with Be (0.57, 1.11, or 3.33 wt.% BeO by aqua regia ICP-AES, QEPMA, and SIMS; Evensen, 1997) were used as standards for the analysis of experimental products. The glasses contained appreciable B, Li, Rb, and Cs (at concentrations far above those estimated for each element in unknowns) and therefore served as standards for the suite of elements in question. All trace elements were further calibrated against the NIST 610 glass, containing nominally ~500 ppm of the elements above (Pearce et al., 1997). The recent analytical assessment of Be analysis by SIMS over a range of geologic materials (Hervig, 2002) shows highly efficient yields of ionized Be and the appearance of only small matrix effects (≪20%). On an atomic basis, working curves for SIMS using mineral, mafic, and felsic glasses (e.g., Ottolini et al., 1993; Shearer et al., 1994; Evensen et al., 1999) show marked convergence with the calibration of this study, which further contains beryllian cordierite (Sponda 454; Armbruster and Irouschek, 1983) as a new crystalline standard. Calibration factors derived from the standards above allowed the normalized count rates to be converted to absolute concentrations. Total internal and external precision (ICP) of BeO analyses of crystals and glass was <3.9%. Data were acquired in three sessions over a 2-yr period. Between these sessions, the working calibration (Fig. 2) and results were highly reproducible (±0.4–2.2%).

4. EXPERIMENTAL PARTITIONING RESULTS AND DISCUSSION

4.1. Potassic and Sodic Alkali Feldspars

Potassic alkali feldspar (K-Afs) forms large euhedral and blocky crystals ranging in length from 25 to 325 μm (relatively megacrystic), and these occur as isolated crystals, glomerocrysts, or crystal networks (Fig. 3a,b). In experiments that included added K-feldspar, those crystal fragments that did not completely dissolve at the preconditioning T are often preserved as cores which facilitated nucleation of overgrowths at the final T step. Between relict cores (showing resorption textures) and thick new overgrowths, a thin zone (2–7 μm) of a Ba-rich component (originating from added Kfs; Tables 3, 4) occasionally occurs; these zones were stabilized at the preconditioning T. K-alkali feldspar hosts inclusions of small melt pools, muscovite (Mus), corundum (Cor), biotite (Bt), magnetite (Mag), cordierite (Crd), phenakite (Phn), or chrysoberyl (Cbr).

Sodic alkali feldspar (Na-Afs: Fig. 3c,d) forms euhedral and blocky crystals (10–60 μm in length) that rarely contain melt pools but commonly contain inclusions of Phn. Few crystals exhibit cores with an increased albite component that survived melting at the preconditioning step and, thus, served as nucleation sites for growth of Na-Afs.

4.1.1. Partitioning of Be

Partition coefficients for K-Afs (Table 5b) show scatter but average ~0.18 in Be-poor systems with no apparent correlation with T. D-values change from 0.18 to 0.14 with increasing T in systems saturated in a Be-mineral. Values of $D_{Be}^{Na-Afs/melt}$ taken
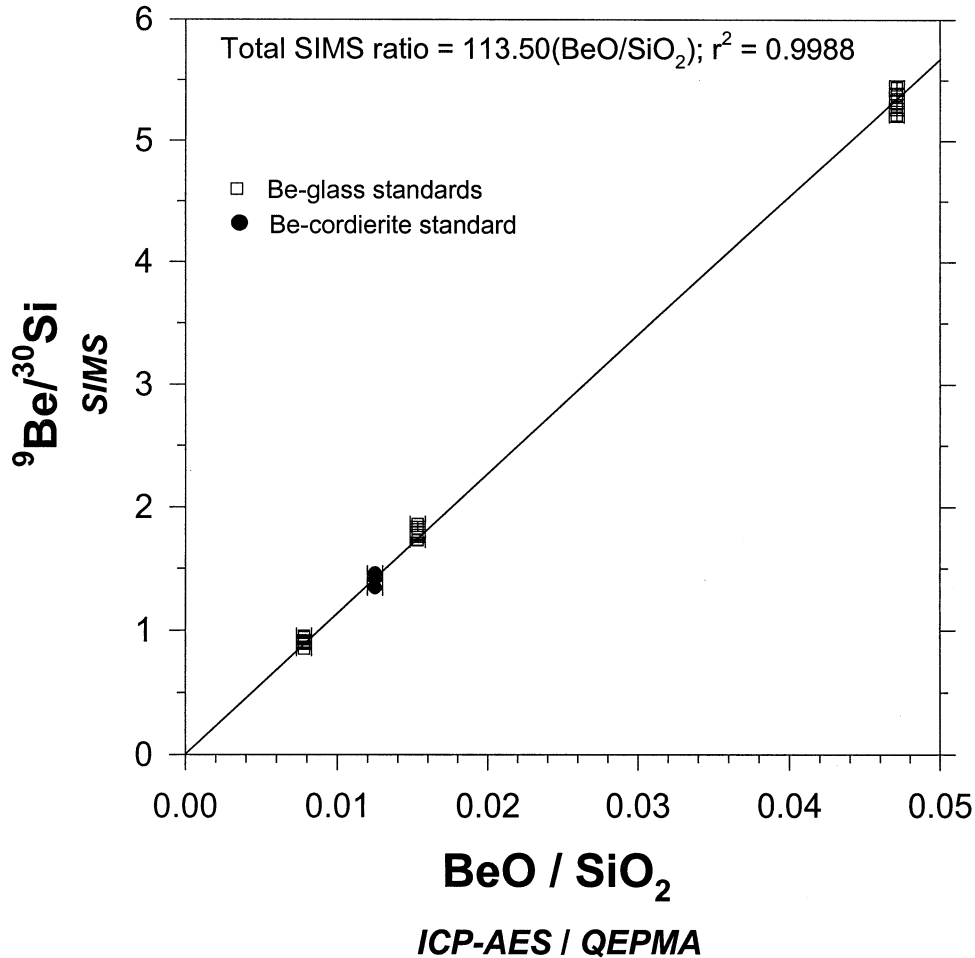
Fig. 2. Working curve for the analysis of Be by SIMS. Analytical techniques are indicated with labels of axes. Nearly 30 data points are shown (most plot on top of each other) from three SIMS sessions over a 2-yr period. Propagated internal and external precision is shown with error bars.

from experiments at 700°C vary from 0.28 to 0.14 for Be-poor and Be-rich melts, respectively (Table 5). Though similar in absolute value, Be appears to be slightly more compatible in sodic vs. potassic alkali feldspar. Unlike K-rich alkali feldspar, sodic alkali feldspar shows a twofold decrease in Be compatibility on beryl saturation.

4.2. Plagioclase Feldspars

Albite (Ab: Table 5) forms euhedral, blocky crystals, ranging from 10 to 525 μm in length, with most crystals ~30 μm in length. In Be-rich melts, albite often contains inclusions of anhedral (partially resorbed) Phn. In experiments that contained grossular, andesine forms euhedral crystals with some skeletal character (Fig. 3e,f). Crystals range from 10 to 125 μm in length. In some cases, fragments of relict albite survived melting in forward experiments. At the lower T step, these fragments become completely armored by new andesine (Table 5), which typically is free of inclusions.

4.2.1. Partitioning of Be

In reversed experiments at 750°C, values of $D_{Be}^{Ab/melt}$ range from 0.10 to 0.37 between Be-poor and phenakite-saturated

melts, respectively (Table 5). Partition coefficients for andesine at 700°C vary between an average of 1.84 (standard error, se = ±0.05) for Be-poor melts and 0.89 for beryl-saturated melts. Andesine is, therefore, the only feldspar in this study in which Be is compatible. This observation suggests that Ca facilitates the coordination environment that accommodates Be, supporting the exchange, $CaBeNa_{-1}Al_{-1}$, in plagioclase.

4.3. Quartz

In the beryl-saturated experiments of Evensen et al. (1999), which were analysed here for partitioning relations, the crystalline assemblage consists of Qtz + Brl + Cbr. In the Be-poor systems utilized in this study, quartz forms nearly equant, euhedral, solid crystals that range from 2 to 50 μm in length. In these melts, quartz crystals occur in distinct networks that transect large areas of crystal-free melt. In beryl-saturated runs, quartz forms larger crystals (10–75 μm) of similar character that coexist with euhedral beryl and chrysoberyl (Fig. 3a,b).

4.3.1. Partitioning of Be

In Be-poor experimental reversals to 800°C, the partition coefficient is 0.24, whereas in beryl-saturated melts, it varies
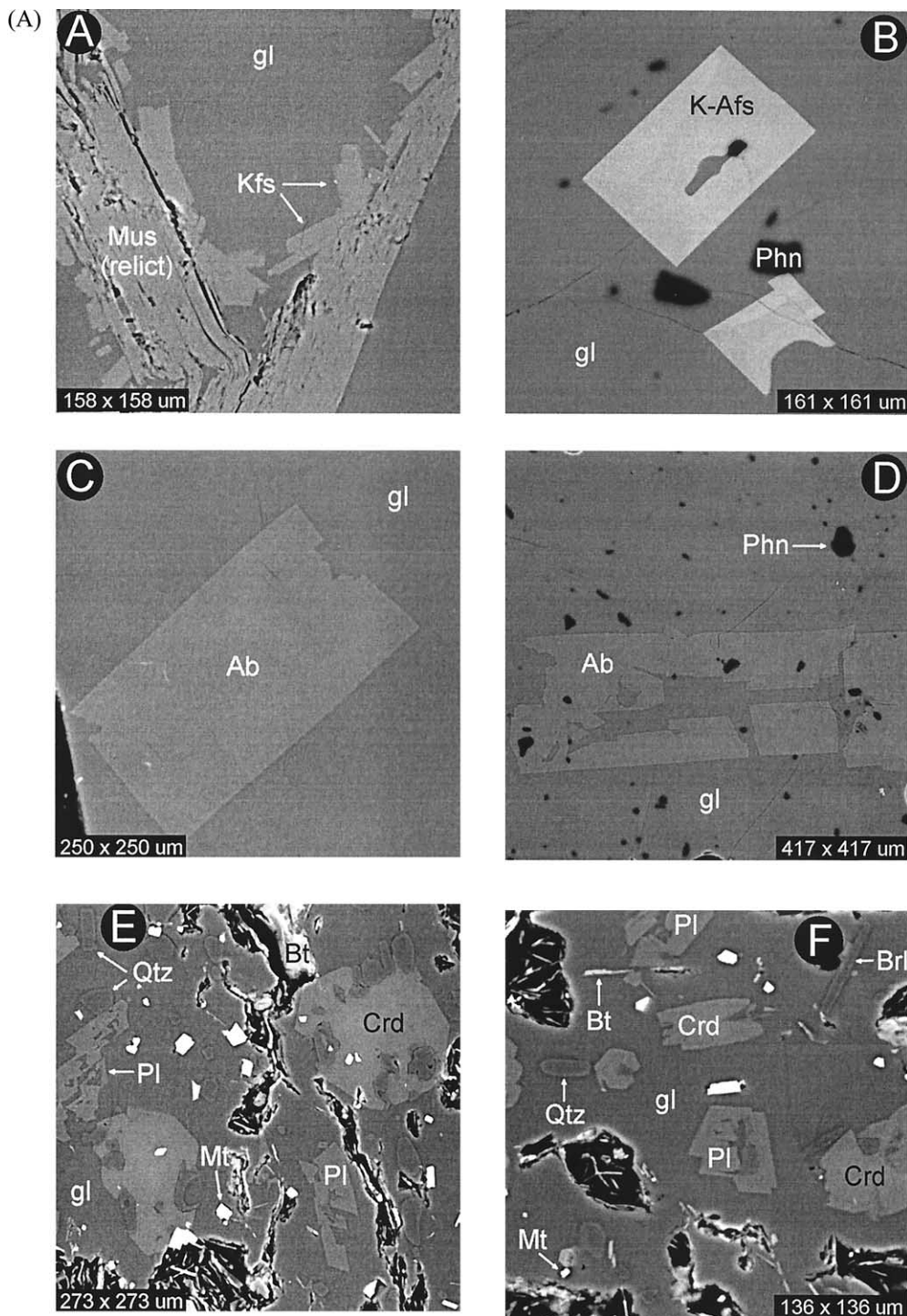
Fig. 3. Backscattered electron micrographs of representative experimental products and assemblages. Image scale is shown in micrometers. Phase abbreviations include: Kfs = K-feldspar, K-Afs = potassic alkali feldspar, Mus = muscovite, Phn = phenakite, Ab = albite, Crd = cordierite, Bt = biotite, Mt = magnetite, Pl = plagioclase, Qtz = quartz, Brl = beryl, Cbr = chrysoberyl, and gl = glass. [A] (a) Reversed experiment BeP-64: K-feldspar crystals grown by reaction 1 (Eqn. 1) from relict Mus in granitic melt that contained trace contents of Be. (b) Reversed experiment BeP-12: K-rich alkali feldspar grown at 750°C from granitic melt saturated in phenakite. (c) Reversed experiment BeP-35: Na-rich alkali feldspar grown at 750°C in Be-poor granitic melt. (d) Reversed experiment BeP-32: Na-rich alkali feldspar grown at 750°C in granitic melt saturated in phenakite. (e) Forward experiment BeP-56: Andesine (Pl) grown by the decomposition of starting grossular in granitic melt containing trace contents of Be. It occurs with the crystalline assemblage Crd + Bt + Mt + Qtz. (f) Forward experiment BeP-53: Andesine grown in a similar assemblage in Be-rich granitic melt, with beryl as a liquidus phase. Beryl shows new growth at low *T* with residual cores from the preconditioning *T*. [B] (a) Reversed experiment BeP-40: New quartz grown at 800°C in granitic melt with trace contents of Be. (b) Reversed experiment Be-75: New quartz grown under
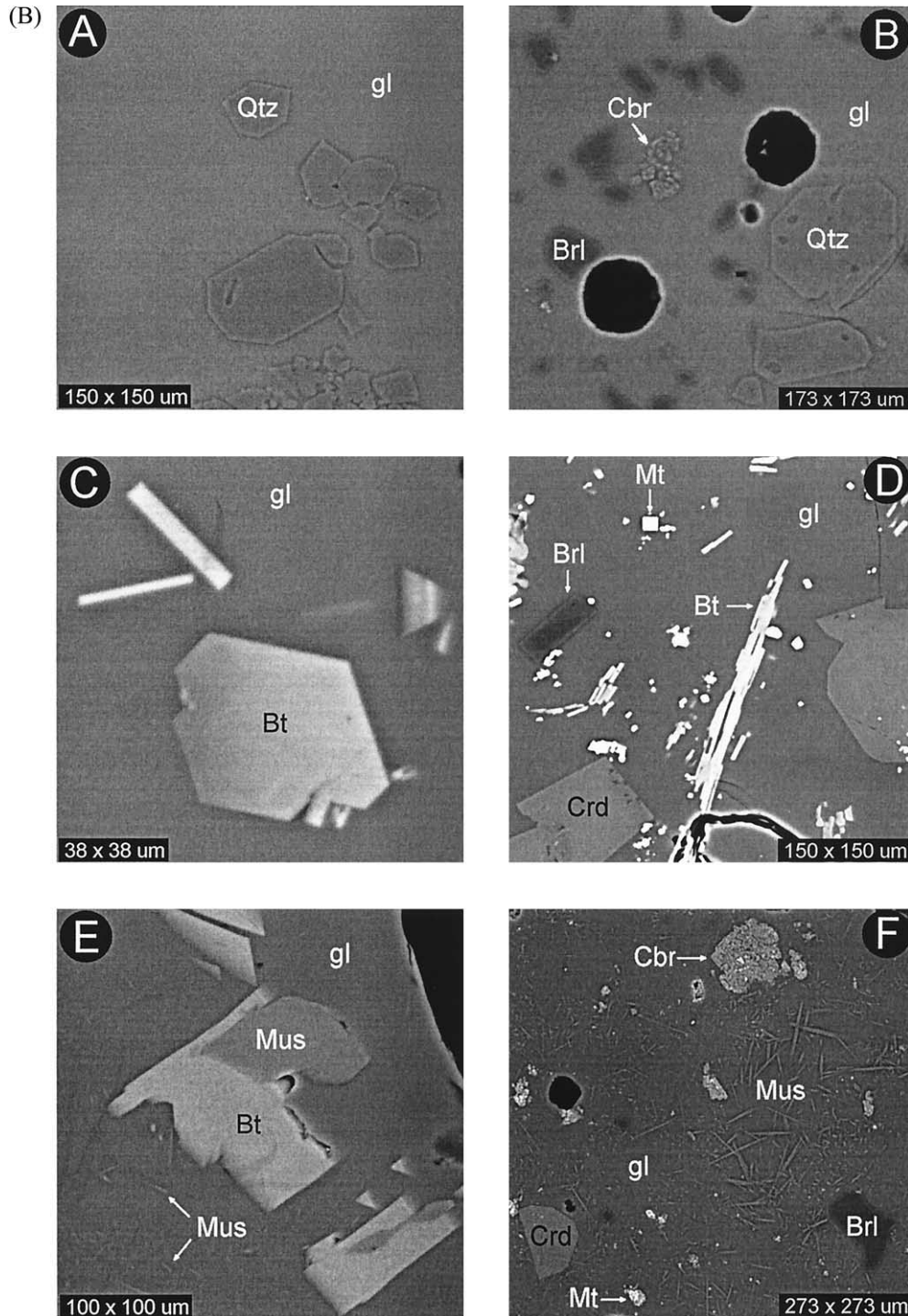
Fig. 3 (continued). beryl-saturated conditions at 800°C. The assemblage contains Qtz + Brl + Cbr in hydrous granitic melt. (c) Reversed experiment BeP-20: New biotite grown at 700°C by reaction 3 (Eqn. 3) in Be-poor granitic melt. (d) Reversed experiment BeP-41: Biotite grown at 700°C in equilibrium with beryl. The assemblage contains Crd + Bt + Mt + Brl in granitic melt. (e) Reversed experiment BeP-47: Coarse muscovite intergrowths with biotite in silicic melt containing Kfs + Mus + Als + Cor + Bt + Mt. Numerous, small crystals of new muscovite are present at lower left. (f) Reversed experiment BeP-52: Abundant muscovite crystals grown in melt saturated with beryl and chrysoberyl; otherwise, this charge contains a similar assemblage as (e).

Table 8a. Experimental Be partition coefficients between rock-forming minerals and silicic melt as a function of temperature.

T (°C)	alkali feldspar		albite	oligoclase-andesine	quartz	dark mica	white mica	cordierite[1]
	K-rich	Na-rich						
				D_{Be} at trace contents of Be				
650						0.42 (0.02)		
675	0.07 -							
680	0.38 -							
700	0.02 -	0.28 -		1.84 (0.05)		0.54 (0.08)	1.35 -	201.21 (0.28)
750	0.26 -		0.10 -			0.39 -		153.06 (4.67)
800	0.19 -					0.52 (0.02)		35.04 (2.31)
850	0.19 -				0.24 -			6.70 -
				D_{Be} at beryl saturation				
675						0.18 -		26.59 (0.43)
680	0.18 -							
700	0.14 -	0.14 -		0.89 -			0.87 -	19.50 (0.62)
750			0.37 -		0.17 -	0.41 -		15.11 (0.22)
800					0.07 -	0.08 -		13.99 (0.45)
850								15.14 (0.48)
900								9.75 -

[1] From Evensen (2001).

from 0.17 to 0.07 from 750 to 800°C (Table 6). These values follow trends similar to other crystalline phases (decreasing with increasing T and with increasing activity of Be).

4.4. Dark Mica

Biotite occurs as both relict and new crystal clusters in most run products (Fig. 3c,d). New biotite is characterized by euhedral, solid crystal forms ranging from 5 to 75 μm in length (commonly ≤10-μm wide). Some crystals host inclusions of magnetite. New crystals exhibit growth in [100] and more magnesian compositions than the starting dark mica (cf. Tables 3 and 7). Relict dark mica is distinguished by coarse crystal size, conspicuous pitting, partly recrystallized crystal rims, and deformed crystal shapes.

4.4.1. Partitioning of Be

Partition coefficients between biotite and melts with trace contents of Be vary from 0.42 to 0.77 (mean = 0.50, se = ±0.04) with no apparent correlation to T (650–800°C; Table 7b). In beryl-saturated melts, these ratios vary from 0.08 to 0.41 (mean = 0.22, se = ±0.10), again, with no correlation to T (675–800°C).

4.5. White Mica

Muscovite occurs in crystal clusters comprised of numerous, small crystals—so numerous that finding Mus-free glass pools for analysis was at times difficult. Muscovite exhibits elongate, sometimes curved, solid crystals 1 to ~60 μm in length. Most crystals are ≪10-μm wide, although there are notable exceptions (Fig. 3e,f).

4.5.1. Partitioning of Be

Partition coefficients for Be between muscovite and melt (Table 7) are 1.35 and 0.93 for Be-poor and beryl-saturated liquids, respectively.

4.6. Cordierite

Evensen and London (1999) show that Be is extremely compatible in cordierite grown from melts of synthetic metapelite composition that contain trace amounts of Be. Partition coefficients range from 202.0 to 6.7 as T increases from 700 to 850°C. As the activity of Be in melt increases, partition coefficients decrease from 26.59 to 9.75 going from 675 to 900°C. However, in the latter case, Be represents a major structural component of cordierite (containing up to 4.4 wt.% BeO; Evensen, 2001).

4.7. Partition Coefficients in Experiment and Nature

4.7.1. Mineral/melt and mineral/mineral partition coefficients

The mineral/melt data of this study are summarized in Table 8 as a function of T. Mineral/mineral values obtained from the same experiments (Table 8) are compared with reported mineral/melt and mineral/mineral partitioning coefficients for natural systems in Table 9. Overall, the ratios from the majority of these systems closely match the experimental D_{Be} values, including those representing evolved, beryl-saturated liquids (Kovalenko et al., 1977). Deviations from the experimental calibration are seen in mineral/mineral values containing plutonic quartz. Because the compositions of coexisting minerals with quartz seem to otherwise converge with experimental partition coefficients, this disparity may possibly reflect some degree of recrystallization of plutonic quartz.

Table 8b. Experimental mineral/mineral partitioning coefficients for Be in granitic melts.

D_{Be}	T (°C)	trace Be 700	beryl-saturated 675	700	750	800
Mus/Kfs		80.96				
Bt/Kfs		29.98				
An32/Bt		4.27		15.18		
Mus/Bt		2.7				
Crd/Bt		17.77–196.9		255.2	38.59	67.42
Crd/Kfs			767			
Crd/An32		118.6		28.19		

4.7.2. Non-Henrian mineral/melt partitioning of Be

The partitioning of Be between minerals and melt becomes strongly non-ideal as Be contents of melt approach saturation in beryl, chrysoberyl, or phenakite in the temperature range of this study. Figure 4 illustrates the shift in mineral/melt partitioning among similar liquid compositions as melts surpass the saturation threshold for a Be phase. Over the same range of T, the partition coefficients fall markedly (except in the case of albite) in the high-Be experiments, indicating that most of these minerals (except in the case of cordierite) become saturated in Be at values in the range of a few tens or hundreds of ppm.

4.7.3. Vapor/melt partition coefficients and vapor transport

Relevant experimentation on F- and Cl-rich evolved silicic compositions (London et al., 1988; Webster et al., 1989) shows that vapor/melt partition coefficients for Be are generally ≤ 1 over a range of fluid compositions, salinities, temperatures, and pressures. Solubilities of Be complexes in equilibrium with Be-minerals are generally far lower (<1 ppm) in aqueous

Table 9. Partition coefficients for Be from natural systems.

Phases	D_{Be} mean (sd)	Data Source
Phenocryst/groundmass of Ongonite, Mongolia		Kovalenko et al. (1977)
K-feldspar/groundmass	0.53 (0.19)	
Albite/groundmass	1.56 (1.46)	
Li-"mica"/groundmass	6.11 (2.76)	
K-feldspar/albite	0.34	
Li-"mica"/K-feldspar	11.53	
Li-"mica"/albite	3.92	
Restite/leucosome Pena Negra, Spain		Bea et al. (1994a)
K-feldspar/leucosome	3.05 (0.3)	
Plagioclase/leucosome	3.13 (0.4)	
Biotite/leucosome	15.5 (0.9)	
Garnet/leucosome	3.23 (0.25)	
Cordierite/leucosome	29.1 (2.1)	
Quartz Monzonite		Beus (1966)
K-feldspar/plagioclase	0.25	
K-feldspar/quartz	2.86	
K-feldspar/biotite	2.00	
Biotite/quartz	1.43	
Biotite/plagioclase	0.13	
Coarse-grained Biotite Granite		Beus (1966)
K-feldspar/plagioclase	2.5	
K-feldspar/quartz	25	
K-feldspar/biotite	0.5	
Biotite/quartz	50	
Biotite/plagioclase	5	
Muscovite granite		Beus (1966)
Muscovite/plagioclase	5	
Muscovite/quartz	250	
Plagioclase/quartz	50	
Coarse-grained "albitized" granite		Beus (1966)
Muscovite/feldspar	2.45	
Muscovite/quartz	49	
Feldspar/quartz	20	
Coarse-grained "Greisenized" Muscovite Granite		Beus (1966)
Muscovite/feldspar	2	
Muscovite/quartz	31	
Feldspar/quartz	16	
Evolved Rhyolitic Dike		Raimbault and Burnol (1998)
Muscovite/groundmass	0.24	
Evolved Rhyolitic Series		G. Morgan and D. London, unpublished data (2001)
Muscovite/biotite	2.10	
Cordierite/biotite	200.1–514.4	
Andalusite/biotite	0.08	
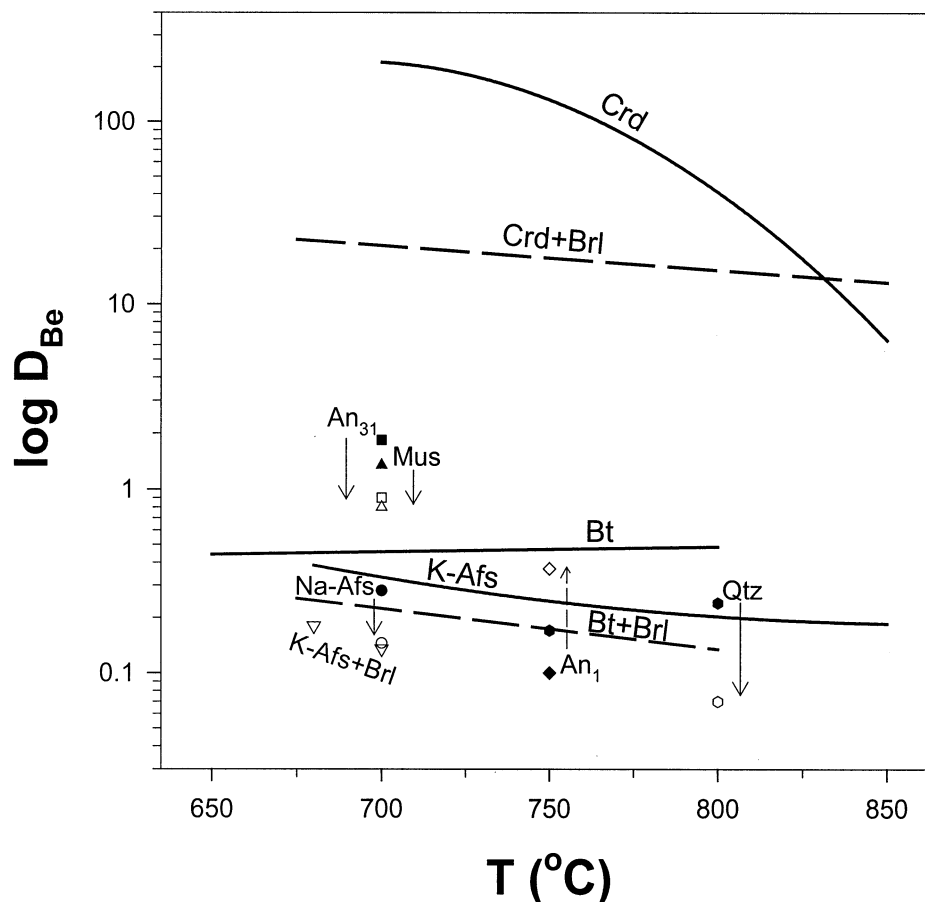
Fig. 4. Mineral/melt partition coefficients for Be in common rock-forming minerals of silicic melts as a function of temperature and activity of Be in melt. Open symbols and dashed lines indicate data from beryl-saturated melts, while filled symbols and solid lines depict melts containing trace levels of Be. Changes from ideality with temperature reveal the non-Henrian behavior of Be partitioning as saturation in a Be-mineral is approached. At similar concentrations of Be in melt, partitioning within certain minerals varies strongly as a function of temperature. The values obtained at trace levels of Be are most relevant to the majority of felsic magmas.

systems (Wood, 1992) than in silicate melts, which are capable of dissolving hundreds to thousands of ppm of Be (Evensen et al., 1999). In regard to the overall budget of Be, silicate melts appear to be more effective agents of transfer than are aqueous fluids. While hydrothermal fluid may still be important in the movement of Be through the crust (e.g., Tatsumi and Isoyama, 1988; Morris et al., 1990; Bebout et al., 1993; Leeman, 1996; Brenan et al., 1998b), it appears that it is less effective than silicate melt on an equal-volume basis.

5. BERYLLIUM SYSTEMATICS IN NATURAL SYSTEMS

5.1. Natural Abundances in Rock-Forming Minerals

To delineate the behavior of Be among rock-forming minerals in crustal systems, we begin by briefly reviewing the typical abundances of Be in these minerals and the means by which Be is incorporated into their structures.

5.1.1. Quartz

Beryllium-stuffed structures of the silica polymorphs are well known, particularly for cristobalite (e.g., Palmer, 1994), in which Na-Be coupling promotes the incorporation of Be.

Quartz in intrusive rocks shows low mean contents of 1.2-ppm Be (Table 1). However, pervasive recrystallization of igneous quartz may be a common phenomenon (e.g., London, 1985), so that the Be contents of quartz phenocrysts quenched in volcanic rocks might give the best indications of the concentrations of Be at magmatic conditions. Unfortunately, a database for Be contents in volcanic phenocrysts of quartz is non-existent, and the disparity between experimental and plutonic quartz cannot be reconciled now.

5.1.2. Plagioclase

The incorporation of Be in plagioclase is probably coupled with Ca via the exchange operator $CaBe^{[4]}Na_{-1}Al^{[4]}_{-1}$. Robert et al. (1995) suggested similar coupling (Ca with Be) for the beryllian brittle mica, bityite, and it is noteworthy that ~60% of all Be minerals contain essential Ca.

Beus (1966) predicted that plagioclase is the chief carrier of beryllium in most crustal rocks. Kosals et al. (1973) found that the mean Be contents of plagioclase in granitic rocks, which varied from An_0 to An_{50}, peak at a maximum of ~11 ppm in calcic oligoclase compositions (~An_{30}). Beryllium decreases

in abundance on both sides of this value, although albitic compositions contain more Be than very calcic compositions. Solodov (1959) noted that beryl-free portions of cleavlandite-rich and albitic aplite units contain from ~2.0 to 4.5 times the Be content of albite in average beryl-bearing pegmatites.

5.1.3. Alkali feldspar

Beryllium likely substitutes into the feldspar structure at tetrahedral Al sites, maintaining charge balance by coupled substitution with alkaline earths, e.g., via $CaBe^{[4]}Na_{-1}Al^{[4]}_{-1}$ in plagioclase (Kosals et al., 1973) and possibly $BaBe^{[4]}K_{-1}Al^{[4]}_{-1}$ in alkali feldspars.

Table 1 shows that potassic feldspar typically contains 3.1-ppm Be and increases in Be content with fractionation to reach values of 7-ppm Be in pegmatitic feldspar. Smeds (1992) found that among pegmatites, the most Be-rich K-feldspar (20 ppm) was found in beryl-undersaturated rocks, whereas lower values (near 10-ppm Be) were characteristic of beryl-bearing pegmatites.

5.1.4. Biotite

Divalent tetrahedral cations are known to enter the mica structure at $Al^{[4]}$ sites by coupled substitution with charge-balancing excess hydroxyl (Ginzburg, 1957). This mechanism, documented in brittle micas, allows for the protonation of apical oxygen of BeO_4 tetrahedra to compensate underbonding at that site (Robert et al., 1995).

With a mean value of 5-ppm Be in granitic rocks, biotite likely carries more Be than Kfs, less Be than white mica, and about an equivalent amount as sodic plagioclase (Table 1). This observation fits with measurements of whole-rock contents of Be in granitoid rocks (Kosals and Mazurov, 1968): Variations are attributed to the presence of biotite and plagioclase. Beryllium compositions of pegmatitic biotite have not been reported. If plagioclase is more calcic than oligoclase, then dark micas should be particularly important reservoirs of Be.

5.1.5. Muscovite

In general, Be appears to be accommodated in white mica via $CaLi^{[6]}Be^{[4]} Na_{-1}Si^{[4]}_{-1}$ (Grew et al., 1986). Going from the brittle mica, margarite, the exchange operator $Li^{[6]}Be^{[4]}Al^{[4]}_{-1}$ leads to the beryllian endmember, bityite, i.e., $CaLiAl_3BeSi_2O_{10}(OH)_2$. However, another vector from margarite, $HBe^{[4]}Al^{[4]}_{-1}$, also appears to be important (J. M. Evensen, D. London, R. L. Hervig, 2002, unpubl. data).

Next to cordierite (and, for example, rarer amphiboles in some alkaline systems), white mica contains the highest Be contents among the rock-forming minerals. Mean contents are ~40-ppm Be (Table 1), although the database is skewed toward pegmatite samples that contain abnormally high contents of Be. White mica in granitic rocks carries a representative mean content of ~25-ppm Be. Muscovite noticeably displays higher Be contents in beryl-absent vs. beryl-bearing pegmatites (e.g., Smeds, 1992).

5.1.6. Cordierite

In cordierite, Be is accommodated in linking tetrahedral sites of Al by the alkali-coupled exchange, $NaBeAl_{-1}$ (Černý and Povondra, 1966) and by the excess silicon exchange, $BeSiAl_{-2}$ (e.g., Baba et al., 2000). These mechanisms vary inversely with temperature: $NaBeAl_{-1}$ at $T < 750°C$ and $BeSiAl_{-2}$ at $T > 750°C$ (Evensen, 2001).

The database is sparse for Be contents of cordierite in silicic rocks, particularly for cordierite-bearing granites (Table 1). The available data, however, indicate that cordierite commonly contains more Be than most other rock-forming minerals. Cordierite from ordinary metamorphic rocks contains ~20-ppm Be. Much higher Be contents have been reported from "cordierites" (e.g., Gordillo, 1979; Schreyer et al., 1979), which probably represent restite from prior partial melting. Cordierite in S-type volcanics from the peraluminous Morococala volcanic suite, Bolivia, contains ~337-ppm Be (G. Morgan and D. London, 2002, unpubl. data). In pegmatites (and the equivalent in granulite facies assemblages, e.g., Baba et al., 2000; Grew et al., 2000), Be contents of cordierite reach weight percent levels. In some cases, pegmatitic Crd may have crystallized at conditions of beryl saturation (Evensen, 2001).

A survey of S-type granite compositions (Evensen, 2001) shows two distinct populations by Be content: Crd-free granites enriched in Be (mean = 6-ppm Be) and Crd-bearing granites depleted in Be (mean = 0.8-ppm Be). Whole-rock beryllium appears to distinguish melts that originated from cordierite-bearing sources (with a depletion in Be by Crd that remains in the source region) from those that originated in deeper environments beyond the stability limits of Crd, for example, in the field of aluminosilicate + garnet.

5.2. Petrological Controls

Partition coefficients indicate that the compatibility of Be (at normally trace levels) in crystalline phases decreases in the order: cordierite $\gg$ calcic oligoclase > white mica > dark mica > albite > alkali feldspar $\cong$ quartz. Hence, the first three or four phases in this sequence control the distribution of Be between restite or crystalline magmatic phases and melt. Among these minerals, Be is compatible in cordierite, calcic oligoclase, and white mica. The positioning of plagioclase in this sequence critically depends on its composition. From estimates (Bea et al., 1994a), it appears that garnet resides approximately near albite in the above sequence.

When cordierite is present, it substantially reduces the Be contents of melt to leave an obvious record in whole-rock values (Table 2). On the other hand, cordierite is the least abundant of these phases. Where cordierite is absent, micas and plagioclase control the Be contents in melt.

5.3. Beryllium at Anatexis

5.3.1. Metapelites at shallow crustal levels: the role of cordierite

When present (e.g., Vielzeuf and Holloway, 1988; Mukhopadhyay and Holdaway, 1993), cordierite controls the Be contents of melts derived from metapelite sources at shallow depths. Cordierite becomes or remains a liquidus phase in many

Table 10. Reported Be contents of migmatite systems Pena Negra Complex, central Spain (taken from Bea et al., 1994b).

Migmatite Facies	Crd-bearing?	Be (ppm)			
		Mean	(se)	Range	n
Mesosome	Yes	2.34	(0.65)	1.13–4.75	5
Melanosome	Yes	6.04	(1.35)	3.51–8.10	3
Leucosome	Yes	1.20	(0.10)	0.37–2.04	6

S-type granite magmas (e.g., Ahmed-Said and Leake, 1990; Ugidos and Recio, 1993; Pereira and Bea, 1994; Bea et al., 1994b), and hence the crystallization of even small quantities of cordierite drives the Be content of melts down to values mostly near 1 ppm.

5.3.1.1. Example: hercynian migmatites of Spain. Table 10 summarizes whole-rock contents of Be in leucosomes, melanosomes, and mesosomes reported by Bea et al. (1994a). Although the starting mesosomes contain average crustal quantities of Be (2 ppm), the melanosomes plainly show enrichment in cordierite-rich restite (6-ppm Be) after melt has been extracted. These derivative partial melts are likely to be minimum to eutectic in composition and potentially represent the composition of the larger fraction of melt available from a given source rock. Represented by leucosomes, these derivative melts are quite Be-poor (1-ppm Be).

5.3.2. Previously depleted metapelitic sources: cordieritites

At equilibrium with cordierite, hydrous granitic melt contains between 0 and 4 normative % cordierite component to temperatures of 850°C at 200 MPa (Evensen, 2001). Therefore, when the mode of Crd becomes greater than a few percent, it likely represents a component of restite.

Cordierite-rich restite, or "cordieritites" (up to 90% Crd in the mode), have been described at several localities (e.g., Gordillo, 1979; Ugidos, 1988; Ugidos and Recio, 1993). Some occurrences even contain beryllian cordierite (Schreyer et al., 1979). Owing to the very high compatibility of Be in cordierite (far higher than for any other major or trace element; Evensen, 2001; London and Evensen, 2001), restitic cordierite should change composition continuously during advancing metamorphic reaction to conserve the most compatible elements. Refractory beryllian cordierite is thereby formed by reaction with melt,

$$Crd = Be\text{-}Crd + melt \text{ (or other mafic phases)} \quad (7)$$
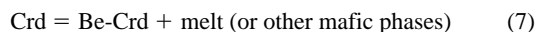
This depletion pathway, which is probably very common in shallow crustal migmatites, illustrates an important concept for the Be budget of melt—Anatexis can separate a low-Be melt from a Be-enriched cordierite residuum—but the cordierite restite in turn represents a potential source of Be if granulite-facies restite is brought to melting conditions (e.g., Grew, 1998; Baba et al., 2000; Grew et al., 2000).

5.3.3. Metapelites at deeper crustal levels: the roles of white mica and plagioclase

Terminal reactions of white mica (Mus = Kfs + Cor + H_2O; Mus + Qtz = Kfs + Als + H_2O) can liberate substantial Be to melt or vapor. Because garnet/biotite + aluminosilicate (+quartz) are stable instead of cordierite, the only notable sink for Be is calcic oligoclase, or biotite to a lesser degree. As long as melting takes place at pressures beyond the stability field of cordierite, then the anatexis of typical metapelites containing white and dark micas, oligoclase-andesine, and garnet (in the place of cordierite) will normally produce melts with the highest initial Be content.

5.3.4. Other quartzo-feldspathic sources: the roles of plagioclase and dark mica

Melts from A-type or I-type sources commonly undergo fractional crystallization with plagioclase and biotite on the liquidus (e.g., Clemens et al., 1986), and these magmas lack (early) muscovite and cordierite. Thus, the accumulation of Be in melt depends primarily on the evolving composition of plagioclase and on the modal amount of biotite crystallizing from the melt. Once the An content of plagioclase falls and restitic biotite is removed, the Be content of I-type or A-type magmas can increase. Černý (1991a, 1991b) has noted that granites with I-type or A-type affinities can produce important Be deposits (beryl in the I-types, beryl or gadolinite in the A-types).

5.4. Beryllium Contents of Silicic Igneous Rocks Worldwide

Table 2 lists reported contents of Be in silicic rocks using 200 mean compositions of granites and porphyries and 1100 compositions of rhyolites for every continent with the exception of Antarctica. Among these, the contents of Be in ppm vary around distinct values of (a) 1 in cordierite-bearing silicic rocks, (b) 4, the mean of all silicic rocks, (c) 6 in S-type silicic rocks without cordierite, and (d) ≥15 in evolved facies of silicic melts. S-type rocks show slightly greater Be contents in relatively unfractionated (6-ppm Be) and evolved facies (20-ppm Be) than do the A-types at comparable degrees of fractionation (4- and 15-ppm Be, respectively). I-type granitoids from convergent settings have lower Be contents (3-ppm Be). The most dramatic feature in this survey is the profound effect of cordierite on the whole-rock abundances of Be.

5.5. Beryllium in Pegmatites: The Role of Beryl

Beryl is the most common Be-saturating phase in pegmatitic liquids derived from parental magmas of all crustal signatures (S, I, A). Depending on the temperature at which crystallization takes place, silicic melts may become saturated in beryl with as little as ∼70-ppm Be (Evensen et al., 1999). Table 11 illustrates the distribution of Be in a schematic pegmatite dike initially

Table 11. Beryllium reservoirs in a schematic pegmatite dike.

Temperature (°C)	700	600	500	400
Be Content of Melt (ppm)	140	60	50	40
Mineral and Mode				
K-feldspar (20%)	27	10	8	6
plagioclase (40%)	258 (An$_{31}$)	14 (An$_1$)	12	9
quartz (30%)	34	7	6	5
muscovite (10%)	189	52	44	34
Total Be in RFM:	137	25	12	8
Be in beryl (% total Be)	1%	75%	76%	80%

Pegmatite Class:	muscovite	beryl	rare-element

```
            ┌────────┐ ┌──────────────────────┐
            │  NO    │ │  BERYL SATURATED      ──▶
            │ BERYL  │ │                       │
            └────────┘ └──────────────────────┘
```

containing 140-ppm Be, which is a typical value for many beryl-bearing pegmatites (London and Evensen, 2002). Here, we used the partition coefficients for trace Be experiments in calculations up to beryl saturation and the Be-saturated coefficients thereafter. If crystallization occurs at 700°C, nearly all the Be in melt (99%) can be accommodated by the rock-forming minerals. These conditions correspond to the muscovite class of granitic pegmatites (Černý, 1991a), which are commonly barren and proximal to their parental granite. The solubility of Be in melt decreases sharply below 700°C (Evensen et al., 1999). On cooling, therefore, beryl saturation is reached at much lower Be contents of melt, and, consequently, most of the Be (nearly 80%) in the dike resides in beryl. This sudden appearance of abundant beryl correlates well with the more distal class of pegmatites, the beryl-type (Trueman and Černý, 1982). At even cooler conditions corresponding to the even more distal rare-element pegmatite formation, beryl hosts the majority of available Be with the remainder dispersed between mainly muscovite and albite. In conclusion, temperature represents the largest control on the distribution of Be among rock-forming minerals, beryl, and melt at the pegmatite stage. We noted that the Be contents of micas and feldspars from barren pegmatites are higher than those from beryl-bearing rocks (Smeds, 1992), which is corroborated by the experimental trends. Although the partition coefficients for Be are generally lower in melts near beryl saturation in our experiments, we suggest that the lower Be contents of minerals, such as mica and feldspar in beryl-bearing pegmatites, stems from their lower temperatures of crystallization (e.g., Morgan and London, 1999) as suggested in the model (Table 11).

5.5.1. Average contents of beryllium

Where the Be contents of pegmatites have been estimated, these range from ~35- to as much as ~575-ppm Be (Table 12; also see London and Evensen, 2002). Beryl is present in most of the pegmatites that contain >~100-ppm Be, and an average Be content for beryl-rich pegmatites lies near 230-ppm Be

Table 12. Average BeO content of granitic pegmatites..

Name and Location	Pegmatite Type (where known)	Average Be (ppm)	Data Source
Tanco Manitoba, Canada	Complex Li - Petalite	163	1
Sparrow Pluton Yellowknife, NWT, Canada	Beryl	260	2
Helen Beryl Black Hills, SD, USA	Beryl	92	3
Tin Mountain Black Hills, SD, USA	Complex Li - Spodumene	223	3
Souchon Kamativi mine, Zimbabwe	Complex Li - Lepidolite	202	4,5
Augustus near Salisbury, Zimbabwe	Complex Li - Lepidolite	202	4,6
Mistress near Salisbury, Zimbabwe	Complex Li - Lepidolite	432	4,6
Benson 1 Mtoko district, Zimbabwe	Complex Li - Lepidolite	577	4,6
Benson 4 Mtoko district, Zimbabwe	Complex Li - Lepidolite	76	4,6
Benson 2 Mtoko district, Zimbabwe	Complex Li - Lepidolite	36	4,6
Al Hayat Bikita district, Zimbabwe	Complex Li - Spodumene	126	4,6
Bikita Main Bikita district, Zimbabwe	Complex Li - Petalite	180	4,6
Unnamed Pegmatite Gobi Field, East Gobi, Mongolia	Complex Li - Lepidolite	155	7
Beryl Rose Darwin district, Zimbabwe		151	4

Data Sources include: 1. Stilling, 1998; 2. Kretz et al., 1989; 3. Staatz et al., 1963; 4. Gallagher, 1975; 5. Rijks and van der Veen, 1972; 6. Ackermann et al., 1968; 7. Rossovskiy and Matrosov, 1974.

Major Pegmatite Zone
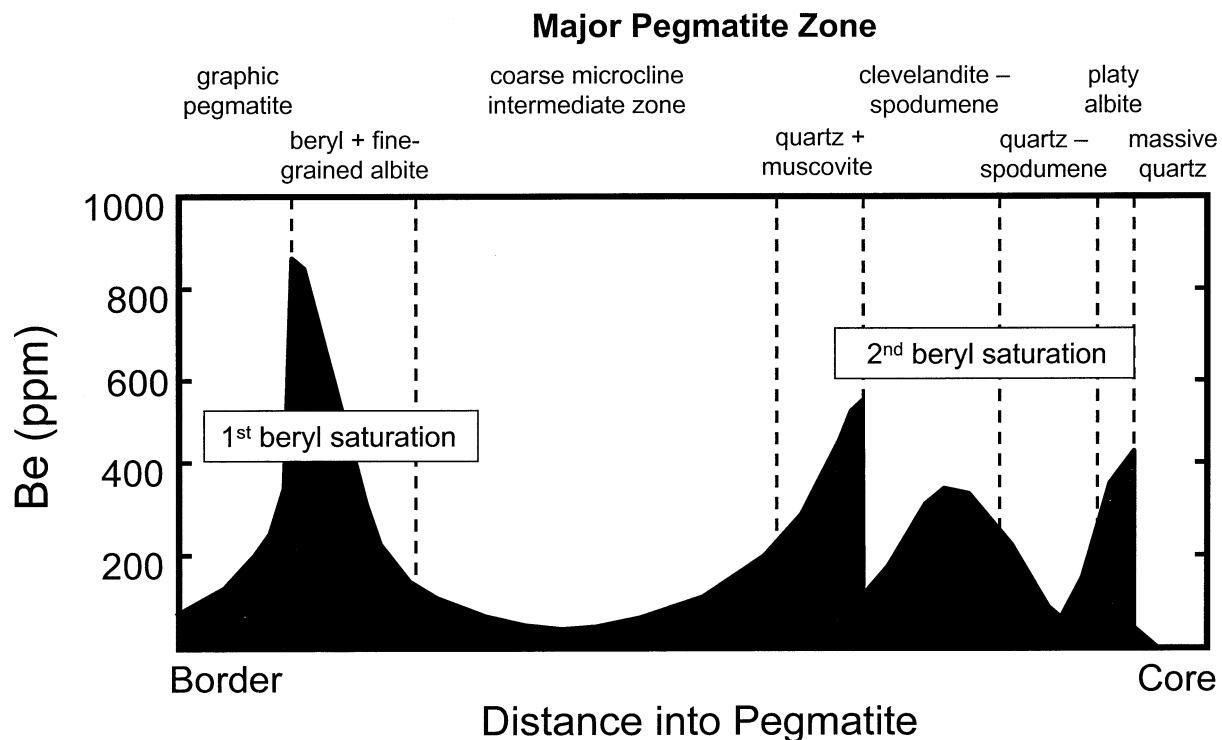
Fig. 5. Distribution of Be within a granitic pegmatite modified after Solodov (1959).

(with considerable scatter; s.d. = 139 ppm). Within pegmatites worldwide, zonation in Be content often occurs as a primary function of two different episodes of beryl saturation. This trend, seen in Fig. 5, stems from the combination of the topology of beryl saturation surfaces and differentiation process with solidification of a pegmatite (Evensen et al., 1999). Cooling gives rise to early beryl at the margins of the pegmatite melt, whereas progressive enrichment at the boundary of the crystallization front (e.g., Morgan and London, 1999) increases with solidification. The latter process may culminate in late beryl saturation within internal pegmatite zones, giving rise to the well-known "beryl fringe" that occurs adjacent to the centralized quartz core.

5.5.2. Wallrock alteration around pegmatites

Because of the inward solidification process that gives rise to pegmatites, two types of wallrock alteration are regularly generated: (1) a localized bulk melt-wallrock interaction on emplacement and (2) typically far more significant alteration zones that mirror the internal abundances of chemically related mineralogy in the pegmatite (e.g., Morgan and London, 1987). While the former alteration style is volumetrically insignificant for most pegmatites, the latter category may result in "blow-outs" that expel highly reactive fluids from pegmatites into wallrock. In this scenario, metasomatic mica generated in the wallrocks should at least partially consume Be carried by pegmatite-derived fluids. Cordierite could be an effective sink as well.

5.5.2.1. Example: the Harding pegmatite, New Mexico, USA.
Wallrock alteration around the large Li- and Be-rich Harding pegmatite—as one of the most beryllian rock bodies on earth (e.g., Montgomery, 1951; Jahns and Adams, 1953), a dramatic example of Be at the pegmatite stage—generated an aureole of alteration assemblages. These contain tourmaline, holmquistite, and epidote in host amphibolites and spessartine, tourmaline, biotite, muscovite, and an Li-poor analog of bityite in altered schists (Jahns and Ewing, 1977; London, 1986; Evensen, 2001). The Li-deficient bityite contains 3.31 wt.% BeO, while coexisting minerals (tourmaline, dark mica, white mica, lepidolite, spessartine) contain from 0- to 10s-ppm Be (J. M. Evensen, D. London, R. L. Hervig, 2002, unpubl. data). It is clear that Be-mica plays an effective role as the sink for Be in this hydrothermal system.

6. THE BERYLLIUM CYCLE IN FELSIC MAGMAS

Crystalline controls on Be geochemistry show that its magmatic cycle becomes a function of three different influences:

- the abundance of quartz, alkali feldspars, and dark mica, which do little to moderate the Be content of granitic melts,
- the composition of plagioclase, and, specifically, the presence of either calcic oligoclase or white mica or both, which constitute important sources or sinks for Be, and
- the presence of cordierite, in which Be is so compatible that solid solutions exist all the way to beryl at high temperature.

In the presence of a crystallizing assemblage of quartz, alkali feldspars, albite, and dark mica, Be behaves as an incompatible

Table 13. Bulk distribution coefficients for Be.

Phase	$K_{Be}^{mineral/melt}$	Normative Weight Fraction	Proportionate $K_{Be}^{mineral/melt}$
Haplogranite minimum at 200 MPa H$_2$O			
Qtz	0.24	0.34	0.08
Ab	0.10	0.38	0.04
Kfs	0.16	0.28	0.04
		$K_{Be}^{eutectic\ assemblage}$	0.16
Muscovite-saturated granite minimum at 200 MPa H$_2$O			
Qtz	0.24	0.33	0.08
Pl (Ab)	0.10	0.37	0.04
Kfs	0.16	0.10	0.02
Ms	1.35	0.20	0.27
		$K_{Be}^{eutectic\ assemblage}$	0.40
Beryl-saturated (pegmatite) granite minimum at 200 MPa H$_2$O			
Qtz	0.17	0.33	0.06
Pl (Ab)	0.37	0.37	0.14
Kfs	0.16	0.10	0.02
Ms	0.87	0.20	0.17
		$K_{Be}^{eutectic\ assemblage}$	0.38

Fig. 6. Schematic representation of the key stages of fractionation for the accumulation of Be in crustal magmas.

element, and its abundance increases rapidly with crystal fractionation. Calcic oligoclase may drop bulk distribution coefficients for Be to near 1. The same is true for white mica. Because muscovite typically constitutes a smaller modal fraction (~10%) than plagioclase, and crystallization normally commences in late magmatic facies, the role of white mica in depleting Be from melt tends to be less than that of plagioclase. Normally, cordierite behaves as a refractory phase during the anatexis of metapelites, and hence it effectively sequesters Be from coexisting partial melts.

Using the experimental database, bulk distribution coefficients are calculated for a model metapelite and model haplogranite system in Table 13. Among the three model rock types, convergence is seen for two K_{Be} values, which illustrates that model metapelitic rocks bearing white mica are just as effective Be sinks as similar rocks at beryl saturation. The per-mineral contribution changes greatly, however, as beryl saturation is attained, which again emphasizes the non-Henrian nature of this system. The bulk values from melts with trace Be are then used in the estimate of Be contents during magmatic evolution from metapelitic to depleted crustal sources, respectively.

Because metamorphic rocks usually arrive at anatectic conditions carrying from 0- to 5-ppm Be in their whole-rock values (Grew, 2002), the anatectic pathway for pelitic to quartzo-feldspathic rocks begins at an average value of 3-ppm Be. In the absence of cordierite at higher pressures (~≥500 Mpa, e.g., Vielzeuf and Holloway, 1988; Mukhopadhyay and Holdaway, 1993), garnet-bearing restitic assemblages will likely exert little influence on the Be contents of melt during anatexis. With a bulk distribution coefficient <1, early partial melts become slightly enriched in Be (4 ppm) as the early mica-rich assemblage begins melting.

Raleigh fractional crystallization (RFC) calculations show that for a melt initially containing 4-ppm Be, crystallization of 80% of the melt yields a concentration of ~15- to 18-ppm Be in melt (London and Evensen, 2002). This value is similar to
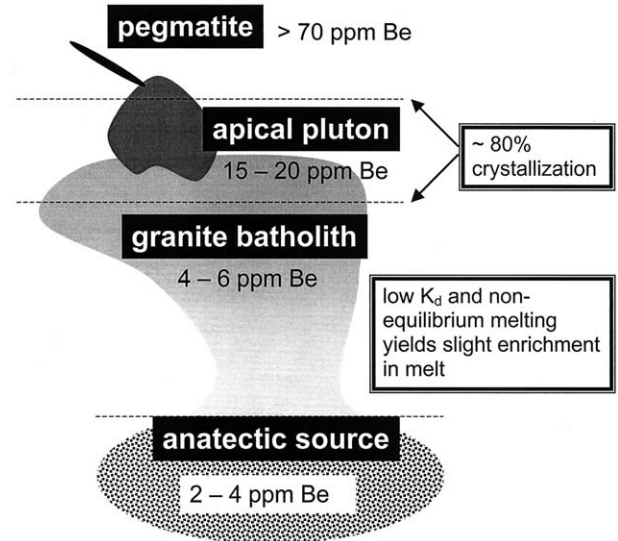
the reported Be contents of small cupolas and dikes of evolved melt (e.g., Luecke, 1981; Shearer et al., 1987; Breiter et al., 1991; Kennen, 2001; see Table 2). When this smaller volume of melt has reached ~80% solidification, then the remaining liquid could possibly achieve beryl saturation, assuming that it could be efficiently extracted to produce pegmatites. Figure 6 illustrates the three-stage process. Kosals and Mazurov (1968) documented variations in Be content throughout a vertically stacked plutonic sequence in Baykalia (primitive to evolved facies to pegmatites). They report mean values of 7-ppm Be in main facies, 10-ppm Be in a slightly enriched facies, and 21-ppm Be in apical apophyses—values that closely parallel the model above.

6.1. Three Principle Pathways for the Budget of Beryllium

6.1.1. S-type magmas with cordierite

If cordierite is present, most of the available Be in the source will be retained in restite, leaving derivative melts highly depleted in Be. This pathway is shown in Fig. 7. Beginning with a whole-rock value of 3-ppm Be, anatexis yields melt containing ≤1-ppm Be (Breaks and Moore, 1992; Bea et al., 1994a; Barbey et al., 1999; see Table 2). Be-enriched restite left behind at the source may later be modified by metamorphism to form higher-grade assemblages from reaction of beryllian cordierite (e.g., surinamite, $Mg_3Al_4BeSi_3O_{15}$ ± taaffeite, $Mg_3Al_8BeO_{16}$ ± Be-rich sapphirine; Grew, 1998). Cordierite is likely to persist as a liquidus phase, although it may decline in abundance or go out as the muscovite or tourmaline consumes the minor (to negligible) femic components present in evolved, low-temperature melts. In evolved melt, the largest fraction of Be will be tied up in white mica, and ~3-ppm Be is likely to occur in melt (or whole rocks). Pegmatites associated with the evolved melts likely contain ~25-ppm Be in their bulk
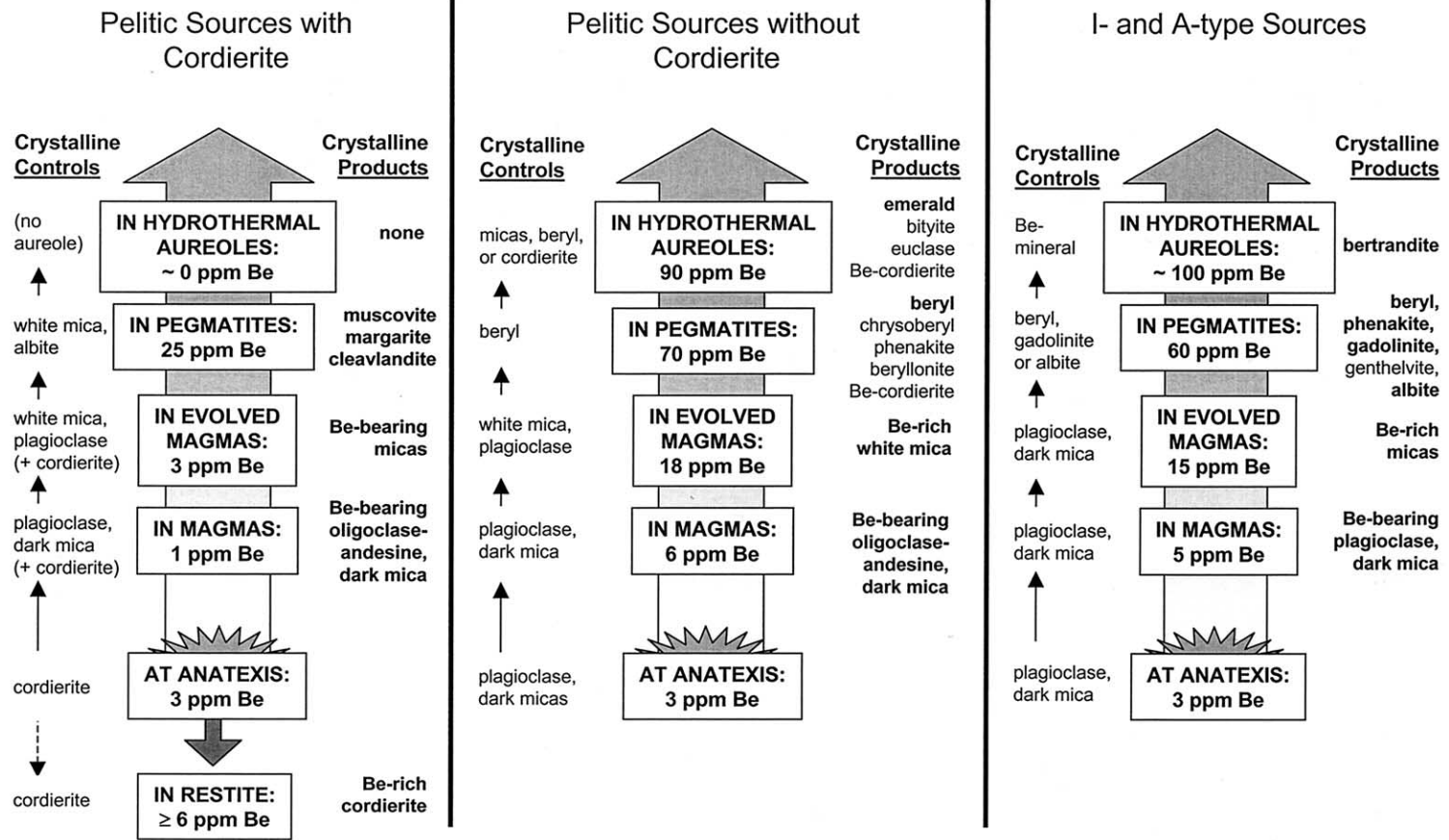
Fig. 7. Three geochemical pathways for Be during the evolution of felsic magmas. The cumulative budget of Be, crystalline controls on Be in melt, and common products in solidified rock are given at successive stages of granitic magmatism.

melts, and here, Be resides mainly in white micas and plagioclase. Hence, these pegmatites will not contain Be minerals.

6.1.2. S-type magmas with garnet

This cycle begins from pelitic source rocks also containing 3-ppm Be (Fig. 7). Anatexis results in about a twofold enrichment of Be in melt (6-ppm Be). Among restitic phases, plagioclase is likely to house the greatest amount of Be. Fractionation then progresses to evolved magmas forming apical plutons. These melts should contain substantial contents of Be. Commonly, 10s up to rarely 100s of ppm Be are observed in whole-rock values of evolved S-type leucogranites (Shearer et al., 1987; Raimbault et al., 1995; Charoy and Noronha, 1996; Zaraisky et al., 1997; Ramirez and Grundvig, 2000; see Table 2). As the Ca content of plagioclase falls with fractionation, white mica becomes the principal sink for Be.

Pegmatites derived from these apical stocks and plutons are predicted to contain ~70-ppm Be in their melts, and thus will probably achieve beryl saturation on cooling to pegmatite temperatures (Evensen et al., 1999). Pegmatitic melts may also reach saturation in chrysoberyl, Be-phosphates, beryllian cordierite, and other Be-minerals. Within a localized aureole (commonly, millimeter to decimeter in scale), metasomatic emerald, euclase, and bityite/beryllian margarite may form in the wallrock alteration assemblage.

6.1.3. I-type and A-type magmas

Figure 7 also follows the Be systematics using the model haplogranite bulk distribution coefficient relevant to I-type and A-type petrogenetic tracks. Sources for these melts likely begin with slightly lower or equivalent contents of Be in whole rocks (3-ppm Be). Enrichment on melting occurs, though to a lesser degree than in garnet-bearing metapelitic source rocks, because of an absence of micas (mainly white mica) in these rock types. Fractionation leading to the melt stage, however, is likely to still be significant with ~5-ppm Be in melt. Plagioclase near the oligoclase-andesine boundary houses the greatest fraction of Be among the rock-forming minerals. In evolved melts that show substantial enrichment of beryllium (~15-ppm Be), increasing sodic plagioclase and dark mica host the majority of Be.

Pegmatites associated with these liquids contain adequate Be to reach beryl saturation at low temperature or at high degrees of fractionation. For instance, in Be-enriched apophyses of some evolved A-type melts, saturation of beryl is achieved on solidification of what is likely to be fractions of 1% (rather than the model 20%) of residual melt. This was likely to be the situation that produced conspicuous "beryl clots" in the late apical leucogranite at Mt. Antero, Colorado, USA (see descriptions by Jacobson, 1993). While occurrences like this may have also been subject to significant cooling to reach beryl saturation, such rocks support the idea that pegmatite-forming melts of this type are likely to be undersaturated (perhaps significantly) with respect to beryl on emplacement.

The styles of mineralization are thus different among these pegmatites (NYF; Cerny, 1991a) and those originating from S-type magmas. Beryl may or may not crystallize in these pegmatites, along with several typical Be-minerals (e.g., gado-

linite group, phenakite, bazzite, helvite group, and behoite). Because the modal proportion of Be-minerals tends to be small in these systems, a significant reservoir of Be ends up in albite whether or not saturation in a Be-mineral is reached. Significant quantities of Be may be available for late hydrothermal alteration, and if aluminous phases are absent in wallrock assemblages, these solutions may become quite beryllian (~100-ppm Be) with, for example, the capacity to precipitate bertrandite.

7. CONCLUSIONS

Beryllium partition coefficients can be used to determine the budget of Be at any stage in a magmatic cycle of the felsic crust. Enrichment of Be will only be achieved in magmas that neither contained cordierite in their source rocks nor large modal proportions of calcic oligoclase as a liquidus phase. Where present, enrichment likely results from either (1) a contribution of white mica at the source or (2) the absence of intermediate plagioclase ± white mica throughout the crystallization interval, so that Be concentrates in residual liquid. Extended fractionation beyond ~95% total solidification by at least a three-step process is required to achieve beryl saturation in granite magmas.

REFERENCES

Ackermann K. J., Branscombe K. C., Hawkes J. R., and Tidy A. J. L. (1968) The geology of some beryl pegmatites in Southern Rhodesia. *Trans. Geol. Soc. S. Africa* **69,** 1–38.
Ahmed-Said Y. and Leake B. E. (1990) S-type granite formation in the Dalradian rocks of Connemara, W. Ireland. *Mineral. Mag.* **54,** 1–22.
Armbruster T. and Irouschek A. (1983) Cordierites from the Lepontine Alps: Na+Be→Al substitution, gas content, cell parameters, and optics. *Contrib. Mineral. Petr.* **82,** 389–396.
Baba S., Grew E. S., Shearer C. K., and Sheraton J. W. (2000) Surinamite, a high-temperature metamorphic beryllosilicate from Lewisan sapphirine-bearing kyanite-orthopyroxene-quartz-potassium feldspar gneiss at South Harris, N.W. Scotland. *Am. Mineral.* **85,** 1474–1484.
Bader R. F., Keaven I. T., and Cade P. E. (1967) Molecular charge distributions and chemical binding. II. First-row diatomic hydrides, AH. *J. Chem. Phys.* **47,** 3381–3402.
Barbey P., Marignac C., Montel J. M., Macaudiere J., Gasquet D., and Jabbori J. (1999) Cordierite growth textures and the conditions of genesis and emplacement of crustal granitic magmas; the Velay granite complex (Massif Central, France). *J. Petrol.* **40,** 1425–1441.
Bea F., Pereira M. D., and Stroh A. (1994a) Mineral/leucosome trace-element partitioning in a peraluminous migmatite (a laser ablation-ICP-MS study). *Chem. Geol.* **117,** 291–312.
Bea F., Pereira M. D., Corretge L. G., and Fershtater G. B. (1994b) Differentiation of strongly peraluminous, perphosphorus granites:

The Pedrobernardo pluton, central Spain. *Geochim. Cosmochim. Acta* **58,** 2609–2627.

Bebout G. E., Ryan J. G., and Leeman W. P. (1993) B-Be systematics in subduction-related metamorphic rocks: Characterization of the subducted component. *Geochim. Cosmochim. Acta* **57,** 2227–2237.

Beus A. A. (1966) *Geochemistry of Beryllium and Genetic Types of Beryllium Deposits.* W. H. Freeman and Company, San Francisco.

Breaks F. W. and Moore Jr. J. M. (1992) The Ghost Lake batholith, Superior Province of northwestern Ontario: A fertile S-type, peraluminous granite—rare-element pegmatite system. *Can. Mineral.* **30,** 835–875.

Breiter K., Sokolova M., and Sokol A. (1991) Geochemical specialization of the tin-bearing granitoid massifs of NW Bohemia. *Miner. Deposita* **26,** 298–306.

Brenan J. M., Neroda E., Lundstrom C. C., Shaw H. F., Ryerson F. J., and Phinney D. L. (1998a) Behavior of boron, beryllium, and lithium during melting and crystallization: Constraints from mineral-melt partitioning experiments. *Geochim. Cosmochim. Acta* **62,** 2129–2141.

Brenan J. M., Ryerson F. J., and Shaw H. F. (1998b) The role of aqueous fluids in the slab-to-mantle transfer of boron, beryllium, and lithium during subduction: Experiments and models. *Geochim. Cosmochim. Acta* **62,** 3337–3347.

Černý P. (1991a) Rare element granitic pegmatites. Part I: Anatomy and internal evolution of pegmatite deposits. *Geosci. Can.* **18,** 29–47.

Černý P. (1991b) Rare-element granitic pegmatites. Part II: Regional to global environments and petrogenesis. *Geoscience Canada* **18,** 49–62.

Černý P. and Povondra P. (1966) Beryllian cordierite from Vezna: (Na+K)+Be → Al. *Neues JB. Miner. Monat.* 1966, 36–44.

Černý P., Chapman R., Schreyer W., Ottolini L., Bottazzi P., and McCammon C. A. (1997) Lithium in sekaninaite from the type locality, Dolní Bory, Czech Republic. *Can. Mineral.* **35,** 167–173.

Charoy B. and Noronha F. (1996) Multistage growth of a rare-element volatile-rich microgranite at Argemela (Portugal). *J. Petrol.* **37,** 73–94.

Clemens J. D., Holloway J. R., and White A. J. R. (1986) Origin of A-type granite: Experimental constraints. *Am. Mineral.* **71,** 317–324.

Evensen J. M. (1997) *Effects of Beryllium on the Liquidus Phase Relations of Haplogranite.* MS Thesis, Colorado School of Mines.

Evensen J. M. (2001) *The Geochemical Budget of Beryllium in Silicic Melts, and Superliquidus, Subliquidus, and Starting State Effects on the Kinetics of Crystallization in Hydrous Haplogranite Melts.* Ph.D. Dissertation, University of Oklahoma.

Evensen J. M. and Meeker G. P. (1997) Feasibility of Be analysis for geologic materials using EPMA. *Microscopy Soc. Am., Proc. Microscopy and Microanalysis* 1997, 3(2), 893–894 (abstract).

Evensen J. M. and London D. (1999) Beryllium budgets in granitic magmas: Consequences of early cordierite for late beryl. *Can. Mineral.* **37,** 821–823 (abstract).

Evensen J. M., London D., and Wendlandt R. F. (1999) Solubility and stability of beryl in granitic melts. *Am. Mineral.* **84,** 733–745.

Gallagher M. J. (1975) Composition of some Rhodesian lithium-beryllium pegmatites. *Trans. Geol. Soc. S. Africa* **78,** 35–41.

Ginzburg A. I. (1957) Bityite-lithium-beryllium margarite. *Mineralogical Abstracts* **14,** 136.

Goldschmidt V. M. (1954) The chemical composition of the cosmos and its various separate mass concentrations. In *Geochemistry* (ed. A. Muir), pp. 69–79. Oxford Univ. Press, London.

Goles G. G. (1969) Cosmic abundances. In *Handbook of Geochemistry,* Vol. 1 (ed. K. H. Wedepohl), pp. 116–133. Springer-Verlag, Berlin.

Gordillo C. E. (1979) Observaciones sobre la petrologı|Aaa de las rocas cordierı|Aaticas de la Sierra de Córdoba. *Bol. Acad. Nac. Cienc.* **53,** 3–44.

Gordillo C. E., Schreyer W., Werding G., and Abraham K. (1985) Lithium in NaBe-cordierites from El Peñón, Sierrra de Córdoba, Argentina. *Contrib. Mineral. Petr.* **90,** 93–101.

Gresens R. L. (1966) Dimensional and compositional control of garnet growth by mineralogical environment. *Am. Mineral.* **51,** 524–528.

Grew E. S. (1998) Boron and beryllium minerals in granulite-facies pegmatites and implications of beryllium pegmatites for the origin

and evolution of the Archean Napier Complex of East Antarctica. *Mem. Natl. Inst. Polar Res., Spec. Issue.* **53,** 74–92.

Grew E. S. (2002) Beryllium in Metamorphic Environments (Emphasis on Aluminous Compositions). In *Beryllium: Mineralogy, Petrology and Geochemistry* (ed. E. S. Grew), *Mineral. Soc. Amer., Rev Mineral.* **48,** (in press).

Grew E. S., Hinthorne J. R., and Marquez N. (1986) Li, Be, B, and Sr in margarite and paragonite from Antarctica. *Am. Mineral.* **71,** 1129–1134.

Grew E. S., Yates M. G., Huijsmans J. P., McGee J. J., Shearer C. K., Wiedenbeck M., and Rouse R. (1998) Werdingite, a borosilicate new to granitic pegmatites. *Can. Mineral.* **36,** 399–414.

Grew E. S., Yates M. G., Barbier J., Shearer C. K., Sheraton J. W., Shiraishi K., and Motoyoshi Y. (2000) Granulite-facies beryllium pegmatites in the Napier Complex in Khmara and Amundsen Bays, western Enderby Land, East Antarctica. *Polar Geosci.* **13,** 1–40.

Hervig R. L. (2002) Beryllium analyses by secondary ion mass spectrometry. In *Beryllium: Mineralogy, Petrology and Geochemistry* (ed. E. S. Grew), *Mineral. Soc. Amer., Rev. Mineral* **48,** (in press).

Huebner J. S. (1971) Buffering techniques for hydrostatic systems at elevated pressures. In *Research Techniques for High Pressure and High Temperature* (ed. G. C. Ulmer), pp. 123–177. Springer-Verlag, New York.

Icenhower J. P. and London D. (1995) An experimental study of element partitioning between biotite, muscovite and coexisting peraluminous granitic melt at 200 MPa (H₂O). *Am. Mineral.* **80,** 1229–1251.

Jacobson M. I. (1993) *Antero Aquamarines: Minerals from the Mount Antero–White Mountain Region, Chaffee Country, Colorado.* L. R. Ream Publishing, Coeur d'Alene, Idaho.

Jahns R. H. and Adams J. W. (1953) Beryl deposits in the Harding pegmatite, Taos County, New Mexico. *Econ. Geology* **48,** 328–329 (abstract).

Jahns R. H. and Ewing R. C. (1977) The Harding Mine, Taos County, New Mexico. *Mineral. Rec.* **8,** 115–126.

Kalt A., Berger A., and Blumel P. (1999) Metamorphic evolution of cordierite-bearing migmatites from the Bayerische Wald (Variscan Belt, Germany). *J. Petrol.* **40,** 601–627.

Kennen P. (2002) The S-type Leinster granite in SE Ireland. In *S-Type Granites and Related Rocks* (ed. B. Chappell and P. Fleming), pp. 65–66, Australian Geol. Survey Org. Record 2001/02 (abstract).

Kosals Y. A. and Mazurov M. P. (1968) Behavior of rare alkalis, boron, fluorine and beryllium during the emplacement of the Bitu-Dzhida granitic batholith, southwest Baykalia. *Geochem. International* 1968, 1024–1034.

Kosals Y. A, Nedashkovskiy P. G., Petrov L. L., and Serykh V. I. (1973) Beryllium distribution in granitoid plagioclase. *Geochem. International* **10,** 753–767.

Kovalenko V. I., Antipin V. S., and Petrov L. L. (1977) Distribution coefficients of beryllium in ongonites and some notes on its behavior in the rare metal lithium-fluorine-granites. *Geochem. International* 1977, 129–141.

Kozlov V. D. (1969) Use of concentrator minerals in evaluation of rarer-element accumulation in the differentiation products of granitoid intrusions. *Geochem. Int.* **3,** 309–321.

Kretz R., Loop J., and Hartree R. (1989) Petrology and Li-Be-B geochemistry of muscovite-biotite granite and associated pegmatite near Yellowknife, Canada. *Contrib. Mineral. Petr.* **102,** 174–190.

Leeman W. P. (1996) Boron and other fluid-mobile elements in volcanic arc lavas; implications for subduction processes. In *Subduction: Top to Bottom*, pp. 269–276. Am. Geophys. Union, Geophysical Monograph.

London D. (1985) Origin and significance of inclusions in quartz: A cautionary example from the Tanco Pegmatite, Manitoba. *Econ. Geol.* **80,** 1988–1995.

London D. (1986) Holmquistite as a guide to pegmatite rare metal deposits. *Econ. Geol.* **81,** 704–712.

London D. and Evensen J. M. (2001) The beryllium cycle from anatexis of metepelites to beryl-bearing pegmatites. In *Eleventh Annual V. M. Goldschmidt Conference*, Lunar Planet. Inst. Contribution 1088, Lunar Planet. Inst., Houston, #3367 (abstract; CD-ROM).

London D. and Evensen J. M. (2002) Beryllium in silicic magmas and the origin of beryl-bearing pegmatites. In *Beryllium: Mineralogy, Petrology and Geochemistry* (ed. E. S. Grew), *Mineral. Soc. Amer., Rev. Mineral.* **48,** (in press).

London D., Hervig R. L., and Morgan G. B. (1988) Melt-vapor solubilities and elemental partitioning in peraluminous granite-pegmatite systems: Experimental results with Macusani glass at 200 MPa. *Contrib. Mineral. Petr.* **99,** 360–373.

Luecke W. (1981) Lithium pegmatites in the Leinster granite (southeast Ireland). *Chem. Geol.* **34,** 195–233.

Lyakhovich V. V. (1977) Distribution of Li, Cs, Be and F in the vertical section of the Element'Dzhurtinsk Massif of porphyritic granites (Northern Caucasus). *Geochem. Int.* **3,** 360–372.

Montgomery A. (1951) The Harding pegmatite—Remarkable storehouse of massive white beryl. *Mining World* **13,** 32–35.

Morgan G. B. and London D. (1987) Alteration of amphibolitic wallrocks around the Tanco rare-element pegmatite, Bernic Lake, Manitoba. *Am. Mineral.* **72,** 1097–1121.

Morgan G. B. and London D. (1996) Optimizing the electron microprobe analysis of hydrous alkali aluminosilicate glasses. *Am. Mineral.* **81,** 1176–1185.

Morgan G. B. and London D. (1999) Crystallization of the Little Three layered pegmatite-aplite dike, Ramona, California. *Contrib. Mineral. Petr.* **136,** 310–330.

Morris J. D., Leeman W. P., and Tera F. (1990) The subducted component in island arc lavas: Constraints from Be isotopes and B-Be systematics. *Nature* **344,** 31–36.

Mukhopadhyay B. and Holdaway M. J. (1993) Cordierite-garnet-sillimanite-quartz equilibrium: I. New experimental calibration in the system FeO-Al$_2$O$_3$-SiO$_2$-H$_2$O and certain P-T-X$_{H_2O}$ relations. *Contrib. Mineral. Petr.* **116,** 462–472.

Newton R. C. (1966) BeO in pegmatitic cordierite. *Mineral. Mag.* **35,** 920–927.

Ottolini L., Bottazzi P., and Vannucci R. (1993) Quantification of lithium, beryllium, and boron in silicates by secondary ion mass spectrometry using conventional energy filtering. *Anal. Chem.* **65,** 1960–1968.

Palmer D. C. (1994) Stuffed derivatives of the silica polymorphs. In *Silica: Physical Behavior, Geochemistry and Materials Applications* (ed. P. J. Heaney et al.), *Rev. Mineral.* **29,** 83–122.

Pereira M. D. and Bea F. (1994) Cordierite-producing reactions in the Peña Negra Complex, Avila Batholith, central Spain. *Can. Mineral.* **32,** 763–780.

Pearce N. J. G., Perkins W. T., Westgate J. A., Gorton M. P., Jackson S. E., Neal C. R., and Cheney S. P. (1997) A compilation of new and published major and trace element data for NIST SRM 610 and SRM 612 glass reference materials. *Geostandard. Newslett.* **21,** 115–144.

Pouchou J. L. and Pichoir F. (1985) "PAP" (ϕ-ρ-Z) correction procedure improved quantitative microanalysis. In *Microbeam Analysis* (ed. J. T. Armstrong), pp. 104–106. San Francisco Press, San Francisco.

Povondra P. and Čech F. (1978) Sodium-beryllium-bearing cordierite from Haddam, Connecticut, U.S.A. *Neues JB. Miner. Monat.* **5,** 203–209.

Povondra P., Čech F., and Burke E. A. J. (1984) Sodian-beryllian cordierite from Gammelmorskär, Kemi 216 Island, Finland, and its decomposition products. *Neues JB. Miner. Monat.* **3,** 125–136.

Raimbault L. and Burnol L. (1998) The Richemont rhyolite dyke, Massif Central, France: A subvolcanic equivalent of rare-metal granites. *Can. Mineral.* **36,** 265–282.

Raimbault L., Cuney M., Azencott C., Duthou J. L., and Joron J. L. (1995) Geochemical evidence for a multistage magmatic genesis of Ta-Sn-Li mineralization in the granite at Beauvoir, French Massif Central. *Econ. Geol. Bull. Soc.* **90,** 548–576.

Ramirez J. A. and Grundvig S. (2000) Causes of geochemical diversity in peraluminous granitic plutons: The Jalmala pluton, Central-Iberian Zone (Spain and Portugal). *Lithos* **50,** 171–190.

Rijks H. R. P. and van der Veen A. H. (1972) The geology of the tin-bearing pegmatites in the eastern part of the Kamativi District, Rhodesia. *Miner. Deposita* **7,** 383–395.

Robert J. L., Hardy M., and Sanz J. (1995) Excess protons in synthetic micas with tetrahedrally coordinated divalent cations. *Eur. J. Mineral.* **7,** 457–461.

Rossovskiy L. N. and Matrosov I. I. (1974) Geochemical features of the topaz-lepidolite-albite pegmatites of the East Gobi, Mongolia. *Geochemical Int.* 1974, 1323–1327.

Russ J. C. (1999) *The Image Processing Handbook*. 3rd Ed. CRC Press, Boca Raton, Florida.

Ryan J., Morris J., Bebout G., and Leeman W. (1996) Describing chemical fluxes in subduction zones: Insights from "depth-profiling" studies of arc and forearc rocks. In *Subduction: Top to Bottom*, pp. 263–268. Geophys. Union, Geophysical Monograph.

Schreyer W., Gordillo C. E., and Werding G. (1979) A new sodium-beryllium cordierite from Soto, Argentina, and the relationship between distortion index, Be content, and state of hydration. *Contrib. Mineral. Petr.* **70,** 421–428.

Shannon R. D. (1976) Revised effective ionic radii and systematic studies of interatomic distances in halides and chalcogenides. *Acta Crystallogr.* **A32,** 925–946.

Shearer C. K., Papike J. J., and Laul J. C. (1987) Mineralogical and chemical evolution of a rare-element granite-pegmatite system; Harney Peak Granite, Black Hills, South Dakota. *Geochim. Cosmochim. Acta* **51,** 473–486.

Shearer C. K., Layne G. D., and Papike J. J. (1994) The systematics of light lithophile elements (Li, Be, and B) in lunar picritic glasses: Implications for basaltic magmatism on the Moon and the origin of the Moon. *Geochim. Cosmochim. Acta* **58,** 5349–5362.

Smeds S. A. (1992) Trace element in potassium-feldspar and muscovite as a guide in the prospecting for lithium- and tin-bearing pegmatites in Sweden. *J. Geochem. Explor.* **42,** 351–369.

Solodov N. A. (1959) Certain regularities of distribution of rare elements in sharply zoned pegmatites (in Russian). *Geokhimiya* **4,** 316–327.

Staatz M. B., Page L. R., Norton J. J., and Wilmarth V. R. (1963) Exploration for beryllium at the Helen Beryl, Elkhorn and Tin Mountain pegmatites, Custer County, South Dakota. *U. S. Geol. Survey Prof. Paper* **297C,** 129–197.

Stilling A. (1998) *Bulk Composition of the Tanco Pegmatite at Bernic Lake, Manitoba, Canada.* M.S. thesis, Univ. Manitoba, Canada.

Tatsumi Y. and Isoyama H. (1988) Transportation of beryllium with H$_2$O at high pressures; implication for magma genesis in subduction zones. *Geophys. Res. Lett.* **15,** 180–183.

Trueman D. L. and Černý P. (1982) Exploration for rare-element granitic pegmatites. In *Granitic Pegmatites in Science and Industry* (ed. P. Černý). Mineral. Assoc. Canada Short Course Handbook **8,** 463–493.

Tuttle O. F. and Bowen N. L. (1958) Origin of granite in the light of experimental studies in the system NaAlSi$_3$O$_8$-KAlSi$_3$O$_8$-SiO$_2$-H$_2$O. *Geol. Soc. Am. Mem.* **74,** 153 pp.

Ugidos J. M. (1988) New aspects and considerations on the assimilation of cordierite-bearing rocks. *Rev. Soc. Geol. España* **1,** 129–133.

Ugidos J. M. and Recio C. (1993) Origin of cordierite-bearing granites by assimilation in the Central Iberian Massif (CIM), Spain. *Chem. Geol.* **103,** 27–43.

Vielzeuf D. and Holloway J. R. (1988) Experimental determination of the fluid-absent melting relations in the pelitic system. *Contrib. Mineral. Petr.* **98,** 257–276.

Visser D., Kloprogge J. T., and Maijer C. (1994) An infrared spectroscopic (IR) and light element (Li, Be, Na) study of cordierites from the Bamble Sector, South Norway. *Lithos* **32,** 95–107.

Webster J. D., Holloway J. R., and Hervig R. L. (1989) Partitioning of lithophile trace elements between H$_2$O and H$_2$O+ CO$_2$ fluids and topaz rhyolite melt. *Econ. Geol. Bull. Soc.* **84,** 116–134.

Wood S. A. (1992) Theoretical prediction of speciation and solubility of beryllium in hydrothermal solution to 300°C at saturated vapor pressure: Application to bertrandite/phenakite deposits. *Ore Geol. Rev.* **7,** 249–278.

Wuensch B. J. and Hörmann P. K. (1978) Beryllium. In *Handbook of Geochemistry, Vol. II(1)* (ed. K. H. Wedepohl). Springer-Verlag, Berlin, 4-A-1 to 4-O-1.

Zaraisky G. P., Seltmann R., Shatov V. V., Aksyuk A. M., Shapovalov Y. B., and Chevychelov V. Y. (1997) Petrography and geochemistry of Li-F granites and pegmatite-aplite banded rocks from the Orlovka and Etyka tantalum deposits in Eastern Transbaikalia, Russia. In Mineral Deposits: Research and Exploration. Where do they meet? (ed. H. Papunen) *Proc. 4th Biennial Soc. Geol. Applied to Mineral Deposits Meeting 1997.* Rotterdam, Balkema, pp. 695–698.